

Center for Accessibility and Safety for an Aging Population

Florida State University

In Partnership with Florida A&M University and University of North Florida

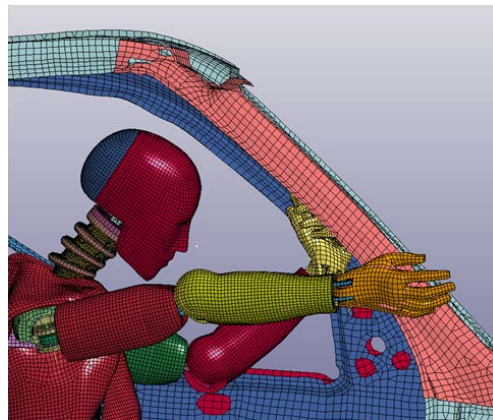
---

## RESEARCH FINAL REPORT

# Biomechanics of Older Drivers in Vehicular Crashes

---

Kakit Fung  
Sungmoon Jung  
John Sobanjo  
Ran Xu  
Jerry Wekezer



[utc.fsu.edu](http://utc.fsu.edu)



**Biomechanics of Older Drivers in Vehicular Crashes  
Final Report**

Kakit Fung  
Doctoral Candidate  
Civil Engineering Department

Sungmoon Jung, PhD.  
Associate Professor  
Civil Engineering Department

John Sobanjo, PhD.  
Professor  
Civil Engineering Department

Ran Xu  
MS Student  
Civil Engineering Department

Jerzy Wekezer, PhD  
Professor  
Civil Engineering Department  
Crashworthiness and Impact Analysis Lab

A Report on Research Sponsored by

Center for Accessibility and Safety for an Aging Population

Florida State University  
in Partnership with Florida A&M University and University of North Florida

December 2016

## Technical Report Documentation Page

1. Report No.	2. Government Accession No.	3. Recipient's Catalog No.	
4. Title and Subtitle Biomechanics of Older drivers in vehicular crashes		5. Report Date December 2016	
		6. Performing Organization Code	
7. Author(s) John Sobanjo Sungmoon Jung Jerzy Wekezer Kakit Fung Ran Xu		8. Performing Organization Report No.	
9. Performing Organization Name and Address Center for Accessibility and Safety for an Aging Population 2525 Pottsdamer St., Suite A 129, Tallahassee FL 32310		10. Work Unit No.	
		11. Contract or Grant No. DTRT13-G-UTC42-033177-036103	
12. Sponsoring Agency Name and Address Research and Innovative Technology Administration 1200 New Jersey Ave., SE Washington, D.C. 20590		13. Type of Report and Period Covered	
		14. Sponsoring Agency Code	
15. Supplementary Notes			
16. Abstract <p>The aging population is expected to increase substantially in the near future. The fatal crash rates (per mile traveled) involving older drivers (65+) are considerably higher than those of younger drivers. Most studies conducted to reduce the crash rate and fatalities of older drivers are non-engineering based approaches. Therefore, these studies could not lead to engineering solutions, such as vehicle design modifications to mitigate injury of older drivers. This study evaluated the mechanics of the aging occupant during an automobile accident. Three different approaches were employed in the study: 1) construction of a simplified dummy and experimental testing, 2) finite element (FE) analysis of vehicle crashes using an FE dummy model, and 3) FE analysis of vehicle crashes using the Total Human Model for Safety (THUMS), which is an advanced FE model of actual humans in detail including the outer shape, bones, muscles, internal organs, etc. Using the first and the second approaches, the effect of driving postures commonly found in older drivers was investigated. Using the third approach, how an accident affects older drivers was investigated. The findings from this study will lead to engineering based solutions to mitigate injury in aging population, which is recommended as future study.</p>			
17. Key Words Add key words here		18. Distribution Statement	
19. Security Classif. (of this report) Unclassified	20. Security Classif. (of this page) Unclassified	21. No. of Pages # of <i>numbered</i> p.	22. Price

Table of Contents

Disclaimer.....	viii
Executive Summary.....	ix
CHAPTER 1 INTRODUCTION .....	1
1.1 Objective .....	1
1.2 Tasks .....	2
1.2.1 Task 1: Key Differences in Older Population.....	2
1.2.2 Task 2: Computational Experiments of Vehicle Crashes .....	3
1.2.3 Task 3: Simplified Physical Dummy Model for Comparison .....	4
1.2.4 Task 4: Aged Human Model through the Modification of THUMS.....	4
1.2.5 Task 5: Computational Experiments of Vehicle Crashes .....	4
CHAPTER 2 LITERATURE REVIEW.....	5
2.1 Driving Posture .....	5
2.2 Anatomical Characteristics of Aged drivers .....	8
2.3 Injury Criteria.....	11
2.4 Dummy Types and Usages .....	13
2.5 Past Research in Using FE for Occupant Safety.....	14
CHAPTER 3 METHODOLOGY .....	16
3.1 Finite Element Simulation .....	16
3.2 Hybrid III dummy .....	21
3.3 THUMS.....	25
3.4 Physical Experiments.....	29
3.4.1 Simplified Anthropomorphic Test Dummy (ATD).....	29
3.4.2 Sled.....	35
3.4.3 Instrumentation .....	41
3.4.4 Experiment Setup .....	42
3.4.5 Data Acquisition and Process.....	46
3.4.6 Experimentation Limitation .....	48
CHAPTER 4 RESULTS AND DISCUSSION .....	49
4.1 Driving Posture Changes due to Aging: Frontal Crash Simulation Using FE49	
4.2 Driving Posture Changes in Frontal Crash due to Aging using Simplified ATD 59	
4.2.1 Head Injury Criteria .....	59
4.2.2 Peak Chest Acceleration.....	65

4.3 Comparison of FE and Physical Test Results .....	69
4.4 THUMS Results.....	70
<b>CHAPTER 5 CONCLUSION/FUTURE WORK .....</b>	<b>76</b>
5.1 Key Findings .....	76
5.2 Recommendations and Future Work .....	79
<b>REFERENCES .....</b>	<b>80</b>

## List of Figures

Figure 3.1 Crash Test Simulation Setup	18
Figure 3.2 Lap Belt Portion Fitting	19
Figure 3.3 Hybrid III 50 <sup>th</sup> percentile dummy model	22
Figure 3.4 Posture angles as defined in (Kyung and Nussbaum, 2009)	23
Figure 3.5 THUMS with Flesh (Left) and without Flesh (R)	25
Figure 3.6 Unmodified Rib Cage (Right) and “Kyphosis” Effect (Left)	28
Figure 3.7 THUMS Simulation Setup with Steering Wheel and Airbag	29
Figure 3.8. Schematic of simplified ATD	30
Figure 3.9 Neck configuration including top disc and bottom block	31
Figure 3.10 Configuration of torso	32
Figure 3.11 Configuration of hip joint	33
Figure 3.12 Configuration of lower extremities	34
Figure 3.13 Configuration of lower extremities	35
Figure 3.14 Main structure of sled rig	36
Figure 3.15 Schematic of impact pendulum	36
Figure 3.16 Simplified dummy and sled rig	37
Figure 3.17 Driving posture angles	42
Figure 3.18 Standardized coordinate systems orientation adapted from (SAE, 2007)	46
Figure 4.1 HIC <sub>15</sub> differences	49
Figure 4.2 Left arm acting as a brace (extended left shoulder simulation)	50
Figure 4.3 Right foot impacting vehicle interior	51
Figure 4.4 Chest acceleration differences	52
Figure 4.5 Spacing between driver’s back and seat back (L) and 2-dof model (R)	53
Figure 4.6 Comparison of chest acceleration between baseline and contracted torso	54
Figure 4.7 Pelvis acceleration differences	55
Figure 4.8 Combination of the previous injury criteria charts	55
Figure 4.9 Triangular plots showing relevant body joints	57
Figure 4.10 Triangular plots comparing young and old postures	58
Figure 4.11 Working environment of Minitab	61
Figure 4.12 Significant factor plot for HIC <sub>15</sub>	62
Figure 4.13 Residual plot for HIC <sub>15</sub>	62
Figure 4.14 Schematic of a standard three-point seatbelt restraint system	65
Figure 4.15 Significant factor plot for peak resultant chest acceleration	66
Figure 4.16 Residual plot for peak resultant chest acceleration	67
Figure 4.17 Comparison of Head Acceleration between THUMS and FMVSS 208	70
Figure 4.18 Comparison of Chest Acceleration between THUMS and FMVSS 208	71
Figure 4.19 THUMS Crash Simulation	72
Figure 4.20 THUMS Head Resultant Acceleration (Single)	72
Figure 4.21 THUMS Head Resultant Acceleration (Combinations)	73
Figure 4.22 THUMS Chest Resultant Acceleration (Single)	74
Figure 4.23 THUMS Chest Resultant Acceleration (Combinations)	75
Figure 4.24 THUMS Chest Deflection (Single)	75
Figure 4.25 THUMS Chest Deflection (Combinations)	76

## List of Tables

Table 1.1 Objectives and tasks	2
Table 3.1 Bodily Joint Angles Used for Simulations	24
Table 3.2 Dimension and material properties of neck discs	31
Table 3.3 Treatment Combinations	43
Table 3.4 Alias structure	44
Table 3.5 Driving posture angles	45
Table 3.6 Channel Frequency Class Reprinted from (Huang, 2002)	47
Table 4.1 HIC <sub>15</sub> values	59
Table 4.1 Peak resultant chest acceleration	65

## List of Abbreviations

Advanced Injury Scale (AIS)  
Anthropomorphic Testing Device (ATD)  
Combined Thoracic Index (CTI)  
Finite Element (FE)  
Finite Element Analysis (FEA)  
Head Injury Criterion (HIC)  
National Highway Traffic Safety Administration (NHTSA)  
Neck Injury Criterion (NIC)  
Total Human Model for Safety (THUMS)

## Disclaimer

The contents of this report reflect the views of the authors, who are responsible for the facts and the accuracy of the information presented herein. This document is disseminated under the sponsorship of the U.S. Department of Transportation's University Transportation Centers Program, in the interest of information exchange. The U.S. Government assumes no liability for the contents or use thereof.

## Executive Summary

The aging population is expected to increase substantially in the near future. The fatal crash rates (per mile traveled) involving older drivers (65+) are considerably higher than those of younger drivers. Most studies conducted to reduce the crash rate and fatalities of older drivers are non-engineering based approaches. Therefore, these studies could not lead to engineering solutions, such as vehicle design modifications to mitigate injury of older drivers. However, this study evaluated the mechanics of the aging occupant during an automobile accident.

This research involved conducting both physical and computational experiments involving dummy models to investigate the biomechanics of older drivers in vehicular crashes. Before conducting these experiments, the concepts of biological changes in older populations needed to be addressed. This allowed us to first find out what makes the older drivers different from younger drivers. It was found that driving posture is one of the two key differences between the two age groups. The Hybrid III computational dummy model and a simplified physical dummy model was used to investigate the effect of driving posture. The other key finding shows that older drivers undergo three changes; material properties changes, compositional changes, and morphological changes. The THUMS model was used for this approach because it has the modification capability to represent an aged driver to be used in the crash simulations.

For both the computational and physical experimentation portion of the posture investigation, we incorporated the idea that driving posture for older drivers tend to be closer to the steering wheel whereas younger drivers are more laid back. All computational work was completed in LS-DYNA; a finite element code used for non-linear impact analysis. The FE simulation was first validated by comparing results with results from the physical crash test of

the same dummy and vehicle models. These results were found in the Federal Motor Vehicle Safety Standards and Regulations Report 208 for Frontal Crash Test. For subsequent simulations, posture changes based on the idea of aging according to literature review were made.

For the Head Injury Criteria, the extended shoulders of an older driver yielded percent differences as high as 16%. The arms act like braces to restrain the torso while the head continues forward. Extending the knees also yielded a 16% increase in head injury. As for the chest acceleration, the extended hip and torso joints showed increased values. It was concluded that sitting closer was beneficial for the Head Injury Criteria but the opposite is true for the chest acceleration. By eliminating the empty space between the driver's back and seatback, the acceleration in the chest remains mainly unchanged. Changing posture does not affect the pelvis acceleration. This investigation gave us a better understanding of what occurs in automobile accidents involving older occupants and ideas for engineering approaches to be undertaken to mitigate injuries.

The physical experiment portion investigated the same concept behind driving posture in terms of only  $HIC_{15}$  and chest acceleration as it was found in the simulation portion that only head and chest accelerations are affected by posture. A simplified anthropomorphic test dummy, sled rig and impact pendulum have been constructed for experiment. Instead of one-at-a-time experiment design, a more efficient fractional factorial design was employed to screen the significant factors that affect  $HIC_{15}$  and peak resultant chest acceleration. The results show that for  $HIC_{15}$ , torso angle, hip angle, right knee angle, right ankle angle, and seatbelt pillar loop anchor location were the significant factors while for peak resultant acceleration torso angle, right knee angle and left ankle angle are significant. Qualitatively, extended torso angle yields both a higher  $HIC_{15}$  value and peak resultant chest acceleration. Lower extremities alter  $HIC_{15}$

and peak resultant chest acceleration asymmetrically. Findings from this helped better understand the biomechanical response of older drivers during car accident and provide useful information regarding safer design of driving compartment for older drivers, including seat and seatbelt, to mitigate their injuries.

The THUMS simulations gave valuable insight on the effects of the aging factors of decreased material property, thinner bone compositional thickness, and kyphosis. For the material property decrease, the chest deflection shows the highest increase. The head and chest accelerations show noticeable increases. For the bone compositional thickness decrease, the chest acceleration shows the highest increase. The head acceleration and chest deflection show noticeable increases. Overall with all three aging factors in place, the head and chest accelerations show high increases. Whereas for the deflection, it remains the same.

The kyphosis effect increases the head resultant acceleration. The effect decreases the deflection of the thorax because the ribs are more in line with the force imposed by the crash. It is able to withstand more force when the ribs are more parallel with the force. As for the chest acceleration, no significant change was present. The accelerometer is placed at the spine. The spine remains in the same position even with the kyphosis effect therefore the acceleration remains the same.

## Chapter 1 Introduction

### 1.1 Objective

The population aged 65 and older is expected to grow in the U.S, from 29 million in 2013 to 53 million in 2030 (Bureau of Labor Statistics, 2013, US Census Bureau, 2012). Many of the older drivers continue to maintain the license, but their fatal crash rates (per mile traveled) begin to increase at age 70 and are considerably higher by age 80 (McCoy et al., 1989). Moreover, drivers 70 and older in 2008 were 3.2 times more likely to die in a crash than middle-aged drivers. A recent study quantified the relation between aging and the chance of dying due to a traffic accident (Kahane, 2013). Most studies conducted to reduce the crash rate and fatalities of older drivers are non-engineering based approaches. These approaches led to non-engineering solutions. One such proposition is placing restrictions on driving privileges based on performance-based criteria such as having adequate visual attention. Another approach is the promotion of self-regulation of driving avoidance for the visually and cognitively impaired older drivers such as avoiding driving at night (Ball et al., 1993, Ball et al., 1998). While these approaches have provided useful guidelines, an underexplored opportunity is to investigate the mechanics behind accidents and fatalities of older drivers.

This goal of this research is to investigate the biomechanics of aging drivers resulted from vehicle crashes. With this knowledge, we can justify a need for engineering-based mitigation methods to be developed to help lessen the injuries that are specific for aging drivers. It is not logical and economical to conduct only physical experiments to obtain adequate data. Therefore, the research relies heavily on finite element method and also a simplified physical experiment of the vehicle crash.

## 1.2 Tasks

This research can be seen as a two-step process. The first step will first quantify the biomechanical changes and differences of older drivers in terms of driving posture changes and anatomical changes. Step 2 will utilize the information obtained in step 1 to run crash simulations to obtain data on the outcome of vehicle crash. For the driving posture changes (first part of the research), the Hybrid III dummy model and a simplified physical dummy model will be used. For the anatomical changes. The THUMS (second part) will used because it allows anatomical changes to be made. The following table outlines the objectives and tasks of this research:

**Table 1.1** Objectives and tasks

Objectives	Tasks	Task Period & Students	Expected Publication
(A) To discover unique characteristics of older population and investigate biomechanics of older drivers through posture changes	(1) To quantify key differences in older population	Jan 2015 ~ Feb 2015 Grad #1 (PhD)	Paper #1
	(2) To conduct computational experiments of vehicle crashes	Mar 2015 ~ Aug 2015 Grad #1 (PhD)	
	(3) To develop a simplified physical dummy model for comparison	May 2015 ~ Aug 2016 Grad #2 (MS)	Paper #2
(B) To investigate biomechanics of older drivers through the modification of THUMS	(4) To develop an aged human model through the modification of THUMS	Sep 2015 ~ Dec 2016 Grad #1 (PhD)	Paper #3
	(5) To conduct computational experiments using the developed model		
(C) To provide recommendations to minimize the severity of injury	(6) To conduct preliminary work on engineering recommendations	Sep 2016 ~ May 2017 Grad #1 (PhD)	Begin Paper #4 (further funding needed)

### 1.2.1 Task 1: Key Differences in Older Population

Drivers and occupants 65 and older show significant changes in terms of their physical anatomy and vehicle interactions. Consequently, they have reduced injury tolerance compared to

the younger population. This task is to find the key differences between older and younger drivers to incorporate into the research in order to discover the biomechanics of older drivers in vehicle crashes. This portion is important part of the research because it dictates the direction where the research follows. The two major key findings between younger and older drivers are driving posture and anatomical differences. The former finding makes use of the Hybrid III dummy model and a simplified physical model while the latter finding makes use of THUMS model. The reasoning behind the choice of dummy models is that posture involves the positioning of the driver while the anatomical changes involve a more detail model such as THUMS.

### *1.2.2 Task 2: Computational Experiments of Vehicle Crashes*

The new FE dummies will enable new discovery in what happens to vehicle crashes of older population. We can conduct virtually unlimited number of computational experiments (i.e., nonlinear FEA) while investigating important parameters of older population.

A validated finite element vehicle model is critical in crash simulation analyses. The National Crash Analysis Center (NCAC) has a database of these validated car models. The model development process follows fairly simple steps. An actual physical car is reverse engineered and modeled to create a computer representation ready for finite element modeling and meshing (Marzougui et al., 2013).

The FE simulation model will consist of the vehicle and dummy models. This particular vehicle model is the Ford Taurus (2001) Modified model and was developed by The National Crash Analysis Center (NCAC) (NCAC, 2014). Its element count was reduced to 28,400 elements from the detailed model of 1 million elements for a shorter run time and less computational power requirement. It has been validated with physical model crash test results.

As for the dummy model, the LSTC Hybrid III 50th Fast Dummy model was implemented in the simulation. This was developed and validated by Livermore Software Technology Corporation (LSTC) (LSTC, 2014). Similar to the vehicle model, it has reduced elements and yields a shorter simulation run time.

### *1.2.3 Task 3: Simplified Physical Dummy Model for Comparison*

This task will create a physical dummy model for the purpose of comparing the FE posture simulation results with physical posture results to solidify the results achieved from the computational experiments. It is both time and cost prohibitive to create a fully dummy model of an aged driver, we will focus on the different driving postures of an aged driver. Therefore, the time and cost to develop the physical dummy model is reduced significantly. The model will have correct mass distribution similar to the human anatomy.

### *1.2.4 Task 4: Aged Human Model through the Modification of THUMS*

An aging person's body undergoes material changes, compositional changes, and morphological changes. The THUMS model is suitable for this task because of its detailed representation of an actual human. Several THUMS models with different combinations of aging factors will be developed to be used in the FE simulations.

### *1.2.5 Task 5: Computational Experiments of Vehicle Crashes*

This task is similar to task 3 but instead of using the Hybrid III, the aged THUMS model will be used in the simulations. A more in depth look at injury will be taken such as bone deformation and chest deflection.

## Chapter 2 Literature Review

### 2.1 Driving Posture

Driving posture is attributed to comfort and discomfort, categorized in either physical or mental comfort. Physical comfort is the comfort we feel based on the positioning of our body and mental comfort is the comfort we feel when we feel safe from having adequate visual of the road, lower driving speed, or vehicle road volume. These attributes dictate the way drivers and occupants sit in an automobile, and in turn dictate the outcome of an accident. The basis of this research comes from the idea that older drivers over age 65+ tend to sit closer to the steering wheel due to conditions such as decreasing eyesight, slower reaction time, and other declines in physical ability (Eby and Kantowitz, 2006, Park et al., 2015).

The driving postures of 90 U.S. drivers, ranged from 20 to 88 years old (with a mean age of 58.9 years old,  $SD=19.8$ ), were measured in a laboratory mockup. Based on the measurements of locations of the 38 landmarks on the body surface and driver mockup, a new set of statistical models was then developed for accurate driving posture prediction with inputs including driver's age, anthropometric dimensions, and driving compartment dimensions (Park et al., 2015).

Another study has been conducted using 38 participants in 3 live driving sessions to simulate driving posture in both sedan and sports utility vehicles. The participants comprised of different age groups and genders. In general, older drivers show smaller angles at the right elbow and hip which indicates that they tend to sit closer to the steering wheel (Kyung and Nussbaum, 2009).

In driving posture, joint angles are bilaterally asymmetric (Hanson et al., 2006b). The left and right sides of the body have different angles. In younger drivers, the angles are assumed to be more extended than that of older drivers, which means young drivers tend to be more laid

back when driving. This first part of the research combines the ideas of driving posture and age found in literature.

There are well established studies conducted on effects of individual bodily regions in terms of variability in driving posture during frontal vehicular impact without the influence of age. One such experiment investigated the effects of posture on the pattern of left-side and right-side hip injuries in offset and angled frontal impact using femurs from cadavers. A total of 35 femur bones were tested in adducted and flexed angle from the neutral hip angle (Rupp et al., 2003). In another similar study, the knee component was investigated. Cadaver knee joints taken from the older population were used to investigate patella subjected to different magnitudes of blunt impact forces. The femur and tibia formed a 90 degree flexed angle with the patella is exposed for impact and injury (Meyer and Haut, 2003).

While these experiments focused solely on individual body parts at the time of crash but that is hardly the case in an automobile accident. The other body parts influence the way a certain body part gets injured. A multi-body musculoskeletal model of a human occupant and driver-side interior compartment of a mid-sized sedan car was used to investigate the influence of pre-collision occupant parameters on injury outcome. The results were taken from numerical simulations. The simulation matrix was designed in such way that it contained the combination of thirteen occupant models with varying stature and mass, twelve muscle activation levels corresponding to completely braced, intermediary levels of muscle contraction, relaxed, and nine occupant driving postures. It was concluded that among anthropometry, muscle bracing level, and seating posture, the latter contributed the most which affecting the overall risk of injury (Bose et al., 2010).

Another study focused on predicting long term injury in the neck portion influenced by seat geometry and comfortable seating posture. The results were taken from numerous numerical reconstructed automobile accidents. Correlations were made in terms of injury, and variations of seat geometry and driving posture (Eriksson and Kullgren, 2006). In another study, the body posture during pre-crash was investigated through the use finite element method. The posture variable in this case differs from the comfortable driving posture mentioned previously. It is the driver's natural tendency to perform evasive movement before the frontal collision. One specific scenario included analyzing the situations where no braking or pre-impact braking occur (Antona et al., 2011).

Similarly, a study assessed the effects of posture change along with pre-impact braking in reducing neck and chest injury risk in frontal impacts (Ito et al., 2012). Aside from the seating posture, seatbelt configuration plays an important role in frontal impact. A survey study of drivers 60 years and older examined the effects of driver characteristics on seat belt fitting. Age and obesity were found to be the biggest influences in seat belt fitting and thus can affect the efficiency of the restraint system during impact (Reed et al., 2013). Obesity can inadvertently cause unnecessary slack in the seat belt by a way of routing the belt further away from the skeletal body structure (Reed et al., 2012). These are just some of the continuing research present in the field of biomechanics but they all lack the effect of age. This leads to the need for knowledge about overall body biomechanics of older driver. The driving posture varies among different age groups but through the manipulation of posture, we can imitate an aged driver to better understand injury difference between the elderly and the younger population. (Yoganandan et al., 2001) focused on hip injury, underscored the importance of leg pre-positioning and the orientation of impact axis when a specific type of trauma to the pelvic region

is produced. Besides neck, spinal alignment has also been proved to be a strong determinant of the biomechanics of cervical spine injury caused by impact.

## 2.2 Anatomical Characteristics of Aged drivers

The concept of modifying a generic finite element dummy model which represents the generic 35-year-old male driver into an “aged” dummy model that can represent the aging driver population, involves intricate modifications to the physiological structure, material properties, and other parameters that define the aging process. To further illustrate the significance of what the research can entail, imagine the idea of having FE models that can account for different age or physiological groups. One study uses an automatic mesh generator to accurately model subject-specific finite element models of femoral bones. The results were verified by comparing FE models to the physical in-vitro samples. The meshes were found to be numerically accurate and similar in weight (Viceconti, 2004). The importance of mesh quality lies not only in skeletal bones but also the skeletal muscles that are attached to them. The mechanical behavior of the skeletal muscles of the human model is considered in two domains that are represented by two separate meshes linked elastically to account for the interaction between the muscle fibers to its extracellular matrix (Yucesoy, 2002). Many research using physical testing have been conducted to determine the effects of aging on the population in terms of physiology and anatomy. In terms of computational methods, the majority of research conducted have been utilizing computed tomography images of elderly bones to automatically generate meshes for use in finite element analysis (Viceconti and Taddei, 2003).

On the other side of the spectrum, experimental data available in literature have been incorporated into modifying parameters to account for age adjustment to develop aged human model. One experiment conducted involved altering the ultimate strain in cortical bones of the

THUMS model for the age adjustment to be used in frontal collision (Forman et al., 2012). The limitation to this would be the dependence on the age related parameters data in literature to be reliable and accurate. Fortunately, the data available on material property changes are abundant and thoroughly investigate but the methods for incorporating said changes in FE model modification are rather scarce. Research have been conducted on the elderly femora bones with 6% lower initial modulus of Elasticity and 10% lower yield stress compared to that of a young adult (Courtney et al., 1996). A simplified approach was taken in order to avoid the difficult tasks of remeshing the entire H-Thorax model to replicate the rib angle change due to aging. This involves placing a force on the sternum with the spine fixed in place while rotating the rib cage until the 9th rib has been rotated approximately seven degrees to achieve the raised rib cage morphologic change that most elderly undergoes. In the same experiment concurrently, two other modifications were implemented to achieve the aging effect; decreasing the material properties of the trabecular and cortical bone and reducing the cortical shell thickness from 5mm to 3mm for all the ribs (Kent et al., 2005b). Another researcher conducted experiments following a similar approach to obtained an aged thorax model and the results were validated with respect to known published data (El-Jawahri, 2010).

Similarly, another researcher changed the material properties of the thorax of the THUMS model to represent an elderly human model to be used in chest compression tests. The properties' values used were obtained from small specimen testing of cortical bones taken from post mortem human subjects (PMHS). The approach was then validated by comparing the results with physical compression chest of the thorax obtained from the same PMHS where the cortical bones were extracted from (Tamura, 2015).

Aside from solely just changing mechanical properties of material, geometric modification approaches were utilized to avoid having to rely on material values obtain from another source. One such study uses the radial basis function (RBF) interpolation using the thin-plate spline as its basis function (Schoell, 2014). This approach can be used to go beyond just modifying specific portions of the body but instead can modify the entire shape of the human body. Also, in addition to RBF, the kriging approach can be used to achieve the same result (Fressmann, 2014).

The original dummy represents the 35 years old male driver. The bones continue to strengthen since birth and plateau at the age of 35, and begin to decrease from that point onwards (Frost, 1997). The cortical bone toughness begins to deteriorate a total of 40% by the age of 100 from 40 years of age. The toughness is characterized using a variable known as fracture toughness ( $K_c$ ) (Nalla et al., 2004). The cortical bones' moduli of elasticity ( $E$ ) decrease by 2.3% per decade from its highest value of 15.2 GPa, the strength (yield stress) decreases 3.7% from its highest value of 170 MPa, and  $K_c$  decreases 4.1% from the highest value of 6.4 MPa (Zioupos and Currey, 1998). The tensile properties of cortical bones indicate that the ultimate stress decreases 5%, and ultimate strain decreases 9% (McCalden, 1993). Linear aging functions have been developed to show the decrease in ultimate tensile stress of cortical bones based on age. Among the different researchers' data, large variations exist among them (El-Jawahri, 2010). In the lower regions of the body, the stress in the post-yield portion and failure strains of the elderly is 20% and 10% less than that of young adults respectively (Yamada, 1970).

The factors that affect injury risks can be linked to three groups: material characteristics, geometric characteristics, and compositional characteristics (Kent et al., 2005b). In terms of compositional changes, the cross-sectional area of the ribs decrease approximately 0.19 mm<sup>2</sup> per year after the age of 25 due to a process known as circumendosteal resorption (Stein, 1976).

### 2.3 Injury Criteria

Bodily injury is often measured qualitatively, visually or by excessive pain; but there are discrepancies as to what really constitute an injury. One person's severe injury may constitute as minor injury for another. Sometimes, injury does not occur immediately after an accident but may occur at a later time. The New Car Assessment Program (NCAP) have developed a quantitative method in the form of injury criteria to determine when an injury has occurred (Hershman and Lawrence). These criteria are computed values using empirical equations that involves change in acceleration and in some cases, change in deflection. NCAP have established known threshold values. Injury occurs if these values are exceeded. These criteria are broken down in different body regions.

The injury criteria were developed by the National Highway Traffic Safety Administration (NHTSA) as a method to quantify injury in occupants in a vehicle crash. These performance criteria represents injury thresholds for certain parts of the body based on the mechanical responses in vehicle crash testing. They are based on the idea that the internal responses of a mechanical structure regardless of size are dependent on the structure's geometry, material properties, and the forces applied to its surface (Eppinger et al., 1999). Human surrogate experiments were conducted to measure parameters and observe their related injury. Then, statistical approaches were taken to derive the injury criteria and threshold values. The injury criteria were developed for the 50<sup>th</sup> percentile male with scaling factors to derive threshold values for the other percentile humans and genders. Currently, aging is not factor in these injury criteria.

In this study, we investigated the Head Injury Criteria (HIC), Chest Acceleration, and Pelvis Acceleration. The pelvis is one of the most fragile areas for the aging human. Hip bones

tend to become brittle in that area, and stress occurs during walking and standing. The injury criteria involve certain parameters such as acceleration, deflection, or force but for this sensitivity study, only the injury criteria involving only acceleration were investigated. We often associate injury with impact that are externally visible but the truth is; injury can occur internally. For example, a human baby should never be shaken because the sudden changes in acceleration can cause internal damage to the head. Modern vehicles perform well in crashes where they can protect the occupants from blunt impact. The vehicle can crumble and absorb the kinetic energy and prevent intrusions from reaching the occupant compartment. However, just sudden stopping can indeed cause extensive damage that are often not externally visible.

Head Injury Criteria is derived by taking the highest acceleration change under the period of 15 msec. The following equation is used to measure the criterion:

$$HIC = \max \left[ \frac{1}{(t_2 - t_1)} \int_{t_1}^{t_2} a(t) dt \right]^{2.5} (t_2 - t_1) \quad (2.1)$$

where  $t_1$  and  $t_2$  are any points of arbitrary time that make up 15 msecs and should result in the highest change in acceleration. Acceleration and time are measured in gravity acceleration ( $g$ 's) and seconds respectively. Initially, NHTSA proposed a period of 36 msecs but based on human volunteer testing, the probability of injury during a longer duration was low. Finally, it was proposed that 15 msecs was the period of time that yields the maximum HIC value. The proposed threshold limit is 700 for both the 50<sup>th</sup> percentile male and 5<sup>th</sup> percentile female.

However, this limit is lower for children. It's based on the assumption that children have different head geometries, material properties, and responses (McPherson, 1980). A scaling technique involving factors for different material properties was proposed. Also, finite element analysis were conducted to come up with lower HIC threshold values for children 3 years and

younger. The adult male threshold limit of 700 encompasses the entire spectrum of age; there is a need for separate values for the aging population due to the decline of bone material properties that occurs at old age.

The Chest Acceleration which is part of the Thoracic Injury Criteria (TIC), is represented by the Combined Injury Index (CTI). Through human surrogate testing, it was determined that injury is caused by both chest acceleration and deflection. The index is determined as follows:

$$CTI = \frac{A_{max}}{A_{limit}} + \frac{D_{max}}{D_{limit}} \quad (2.2)$$

It is computed by taking the sum of maximum acceleration over acceleration limit and maximum deflection over deflection limit. Focusing solely on the 50<sup>th</sup> percentile male, the index limit is 1.

The index value is lower for 5<sup>th</sup> percentile female and children. The acceleration limit and deflection limit is set as 90 g's and 103 mm respectively. These two values are only to be used in determining the CTI while individually, there are lower. The individual values for acceleration and deflection are 60 g's and 63 mm respectively.

For both frontal crash and side impact scenarios, the pelvic injury criteria is defined in terms of force rather than acceleration (Salzar et al., 2006, Leport et al., 2007). However, for the of side impact, pelvic acceleration is an additional injury criterion. Its threshold value is 130 g's. In the case of frontal crash, there isn't an acceleration associated injury criterion but for the focus of our study, the pelvis acceleration was considered.

#### 2.4 Dummy Types and Usages

The FEA of vehicle crash for general population is well established because the standard dummies are based on average of the entire population (Humanetics, 2014a). Various FEA dummy models exist such as LSTC\_NCAC Hybrid III 50<sup>th</sup> Dummy (Guha, 2013), which is a computational model of a physical dummy corresponding to an average male (Humanetics,

2014b). Examples of other Finite element (FE) dummies are female (Kimpura et al., 2005), a pregnant woman (Moorcroft et al., 2003), and a three-year old child (Mizuno et al., 2005).

On the other hand, only limited studies have been conducted on the FEA of older population. An elderly female 5<sup>th</sup> percentile FE dummy was successfully developed based on the Total Human Model for Safety (THUMS) by scaling the model and implementing aging effects in material properties such as the decrease in physiological cross-sectional area (PCSA) of muscles and the decrease in tensile stress in bones that plague the aging population. The ratio of muscular PCSA of an aging female to a young male ranges from 13% to 84% with an average value of 51%. The fracture stresses and strains for the aging people show a consistent 20% and 10% less than the younger population respectively (Iwamoto et al., 2010). In another finding, a 50<sup>th</sup> percentile young and elderly male thoraxes was developed from the Ford Human Body Model (FHBM) which represents a 53-59 year old male. The results show that the newly developed 75 years-old male has a fracture stress value of 123MPa compared to 145MPa that of a 35 years-old male (El-Jawahri et al., 2010).

### 2.5 Past Research in Using FE for Occupant Safety

Toyota Collaborative Safety Research Center (CSRC) is in the progress of scanning an elderly female (65 to 75 year old) body for the development of a virtual geometry identical elderly female for FE model meshing for future aging population research (Center, 2011). With that in the process of development, certain issues still exist that need to be addressed; the variability of weight (obesity) and gender related factors aside from the aging aspect. The University of Michigan Transportation Research Institute (UMTRI) has developed framework for developing a parametric human FE model which can automatically adjust and recreates itself according to the parameters given such as age, gender, and body mass index (Hu et al.,

2012). Thus, this can help overcome the variance in different aging population samples.

Focusing on the morphological changes in the thorax region, Generalized Procrustes Analysis (GPA) was conducted on computed tomography (CT) image data of 63 individuals to develop shape change coefficients. This enables the development of scalable thorax shapes for a number of different ages (Gayzik et al., 2008). These findings can prove to be a helpful tool in modifying generic FE dummy models into elderly ones (Gayzik et al., 2006).

## Chapter 3 Methodology

### 3.1 Finite Element Simulation

The computational experiments were conducted entirely in finite element (FE) environment and they relied heavily on the usage of the dummy and vehicle models. Therefore, it was important that suitable models were used. These dummy models are available in different sizes and genders and are based on physical anthropomorphic test devices (ATD). These ATDs are available in different sizes and genders based on the population percentile (Maurath and Guha, 2010). For physical crash testing, the male Hybrid III 50<sup>th</sup> percentile dummy is used for its excellent biofidelity and result outputs. This particular model represents the largest group of drivers in terms of size and gender. Therefore, this particular dummy model was the focus of the research. The FE dummy counterpart was developed by Livermore Software Technology Corporation (LSTC) and the National Crash Analysis Center (NCAC).

Next was the vehicle model that can accommodate the dummy. The first requirement was that the dummy has to fit realistically inside the compartment with adequate space to allow angle changes later in the experiment. The second requirement was that it should not contain too many elements that would result in long computation run times. The vehicle elements shouldn't be finer than the dummy model elements and should be fine enough to produce accurate results because the main focus is on the dummy and its outputs. The experiment could have been done in a crash sled setup but to better simulate a real crash, an actual vehicle model would be ideal. The selection of vehicles was limited to the availability of the vehicle models in the National Crash Analysis Center online library database. These models were modeled to virtually represent the actual vehicles and validated according to their response in a crash. The selection of the 2002 Ford Explorer model were based on those aforementioned requirements and for its robustness.

The physical vehicle was disassembled into different parts classified by material type. The parts were scanned for their geometry and thickness. Unknown parts were given standard material types such as steel with standard values of strength and modulus. All vehicle parts were included with the exception of steering wheel and column, door trim, and rear seat cushions. Accelerometers were included in the model to measure accelerations in the vehicle. The resulting vehicle model consists of 714,205 elements which comprise of shell, beam, and solid elements (Marzougui et al., 2012). The vehicle model was validated by comparing crash test results from an actual Ford Explorer with two Hybrid III dummies in the driver and passenger compartment. The results from the FE simulation were fitted with the results from the physical crash test. Accelerations from the left and right rear seat crossmembers and engine top and bottom were compared. The values matched closely. Besides comparing data results, the vehicle model was also checked for intrusion damage. The FE model was further validated by Canadian rigid wall impact, side impact, and offset deformable barrier tests. The model was checked for robustness by having the vehicle impact into a pole to induce large deformations.

The preprocessor LS-PrePost was used for the entire investigation. The basis for the simulation keyword was the Hybrid III 50<sup>th</sup> percentile dummy keyword downloaded from LSTC database. The dummy model consists of 256 beam, 226,452 shell, 225,638 solid elements. The vehicle model was then imported with part numbering offset into the keyword deck. Consistent units of kg, mm, and secs were used. The combined keyword file was renamed "simulation" for convenience. The simulation as shown in figure 3.1 was setup according to the Federal Motor Vehicle Safety Standards and Regulations (FMVSS) no. 208 for 2002 Ford Explorer. It contains detailed information and results on the physical frontal crash testing of said vehicle (Ivory and Richardson, 2001). The ATD used in the testing was the physical counterpart of the Hybrid III

50<sup>th</sup> percentile FE dummy. The reason for following the report closely was to arrive at a validated simulation that would be used in following simulations. The FMVSS no. 208 report consists of standards used to assess new vehicles in frontal crashes by the NCAC.

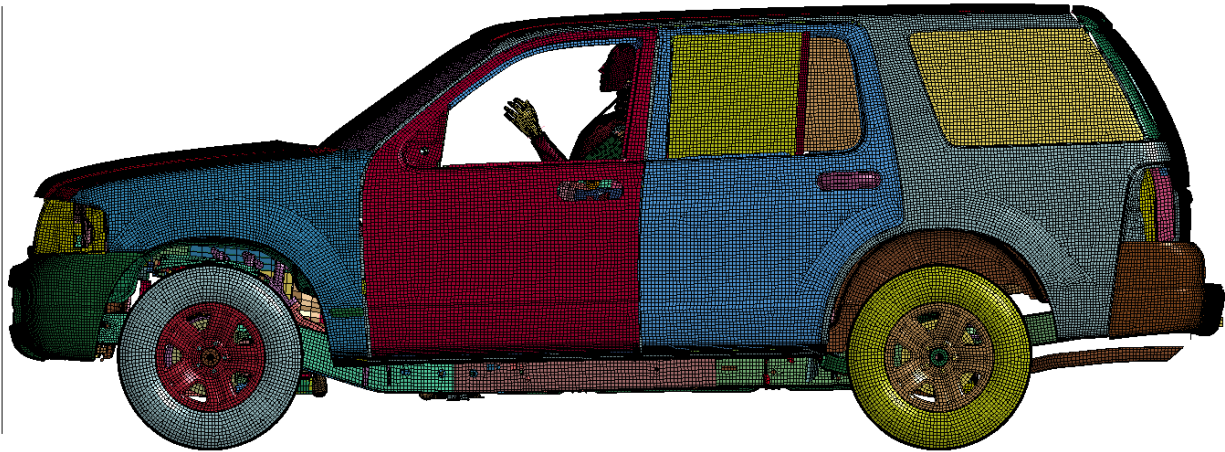


**Figure 3.1** Crash Test Simulation Setup

The biggest discrepancy between the physical vehicle and the finite element model was the nonexistence of the steering wheel and column, and airbag in the FE model. These missing components made the validation process difficult because during a frontal crash, the dummy will impact the airbag deploying out of the steering wheel. This will affect the head injury criterion greatly. As a result of this setback, the validation stage and later simulations showed higher HIC values. Creating a steering wheel with airbag model would proved to be difficult because manufacturers do not share their proprietary information such as airbag deployment time which makes a huge difference in results. To address this, more emphasis was placed on the other chest and pelvis which are not in direct impact with the airbag.

A three-point seatbelt was created and fitted onto the dummy. The seatbelt fitting was done through “Beltfit” keyword function in LS-PrePost. The seatbelt used was a mixed seathbelt that consisted of shell elements connected with Constrained Nodal Rigid Body (CNRB) to beam

elements. The beam elements were anchored to the vehicle. A seatbelt can only provide in-plane resistance so the shell element formulation was set as Belytschko-Tsay membrane element. This formulation allows only in-plane stiffness whereas traditional shell elements provide both in-plane and out-of-plane stiffness.

The fitting took numerous attempts to implement due to the limited information given in the report. The beltfit function requires a minimum of two points to form a belt, from the information given in the report, it was possible to come up with three points to fit the shoulder belt portion. The midpoint of the belt was determined to be 307.5 mm above of the top of the leg. The midpoint for the lap belt was determined as follows: the Z coordinate was the middle point between the top of the hip block and top of the leg and the X coordinate is the middle point between the legs. Figure 3.2 illustrates the location.

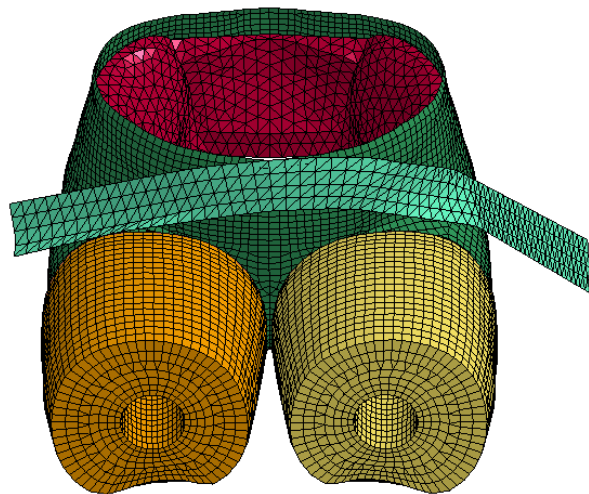


**Figure 3.2** Lap Belt Portion Fitting

The shoulder belt portion was looped through a slipping to form the lap belt portion. This was accomplished by first creating the shoulder belt and lap belt portions using the last node of the shoulder belt as the first node of the lap belt. That node was duplicated and formed as the

slipping node. This allows the seatbelt beam elements to slip through the node to prevent excessive deflection in the torso and hip. The offset used in the belt fitting was 1 mm from the surface of the dummy. The thickness of the torso jacket was 0.01 mm while the thickness for the pelvis block was 6 mm. This caused a problem with excessive slack in the seatbelt. This was solved by first decreasing the thickness of the pelvis down to 0.01 mm and then recover the pelvis thickness after the completion of seatbelt fitting. The belt's loading and unloading curves were created as a near linear curve reaching a value of 10 newton at 6% percent strain. The location of the belt was adjusted several times until the belt restrain the dummy that yielded matching results. This belt setup was kept the same for the simulations that were to follow. For certain posture changes, the belt had to be altered to conform to the shape of the body but the anchor points were kept the same at the same locations.

After the primary setup, contact between the dummy and vehicle needed to be established. The Automatic\_Surface\_To\_Surface contact card was used. The “automatic” always considers thickness offsets and has no segment orientation which allows it to consider both directions. The “SOFT” parameter was set to 1 for contact between soft materials (e.g. dummy) which prevents negative volume errors. The FMVSS No. 208 regulation requires the vehicle velocity to be 30 mph at the time of impact for a frontal barrier impact test. However, in this particular FMVSS No. 208 report, the impact velocity was 35 mph. Therefore, in favor of controlled comparisons, the impact velocity for the baseline and subsequent simulations was set to be 35 mph. Unlike the robustness of the vehicle model, the dummy needed more attention. Initially, the simulation terminated prematurely due to dummy solid elements experiencing negative volumes. This occurred to the large large deformations induced by high velocities. The vehicle model comprised of metal parts that deform under high force while the dummy model

comprised of deformable parts susceptible to deformation. Proper handling of the hourglass type for the dummy parts was required. The solid elements experiencing negative volumes errors were changed to type 5 Flanagan-Belytschko which forms stiffness with exact volume integration.

### 3.2 Hybrid III dummy

The Hybrid III dummy model is a finite element representation of the physical ATD. It was developed by reversed engineered the physical ATD and scanned it for part geometry. Once all the parts were scanned, the image data was imported into a pre-processor for mesh generation. The result is a computational version of the physical model as shown in figure 3.3. The element size were taken as 6mm to provide good interaction with seat constraints and vehicle. The FE model was developed in such a way that it mimizes difference between the FE model and actual physical dummy. The physical dummy flexible components were modeled as deformable components. The non-deformable steel components were modeled as elastic material type 1 in LS-DYNA. The dummy's polyvinyl skin was modeled as visco-elastic material type 6. The foam and rubber components were modeled as Blatz-ko rubber type 7 and viscous foam type 62 respectively. The dummy weighs 79kg and 5'-9" upright height which represents the average 35 year old male (Mohan et al., 2010).

The dummy model was calibrated to fully imitate the physical crash test dummy through the Head Drop, Neck Extension, and Thorax impact certification tests under the Code of Federal Regulations Title 49, Part 572 subpart E. The head was dropped at a height of 376 mm where the forehead made contact with a rigid plate. The resulted peak acceleration was within the defined value based on the dummy size. The neck was developed to express human-like dynamic motions of flexion and extension response that would occur to a human driver in a crash. The

upper torso was developed with a special damping material that can undergo force-deflection characteristics. The dummy was seated on a flat surface with its upper and lower legs placed horizontally on the surface. Then, the thorax was subjected to an impact of a swinging pendulum. The resulted peak force was within the defined value based on the dummy size.

With these features, this dummy model is excellent for driving posture changes. Its torso, hips, and limbs are rotatable and articulated. It is not as detailed as the THUMS model which is used for in depth investigation of anatomical changes and human biomechanics but it provides the adequate functions and outputs.



**Figure 3.3** Hybrid III 50<sup>th</sup> percentile dummy model

To start off dummy positioning, the “H-point” needs to be determined. The “H-point” is essentially the hip joint at which the torso rotates about. It is different from the center of gravity of the dummy. The positioning tree script provided within the dummy model keyword file

allowed the translation of the dummy by the H-point. The test dummy position measurements found in the FMVSS report was used to determined the H-point. Not all of the measurements were needed since the vehicle FE model did not have steering wheel, steering column, and acclerator pedals. Initially, it was also found that the seat in the FE model was further towards the back of the vehicle so many measurements given by the report were irrelevant but they did provide an approximate position.

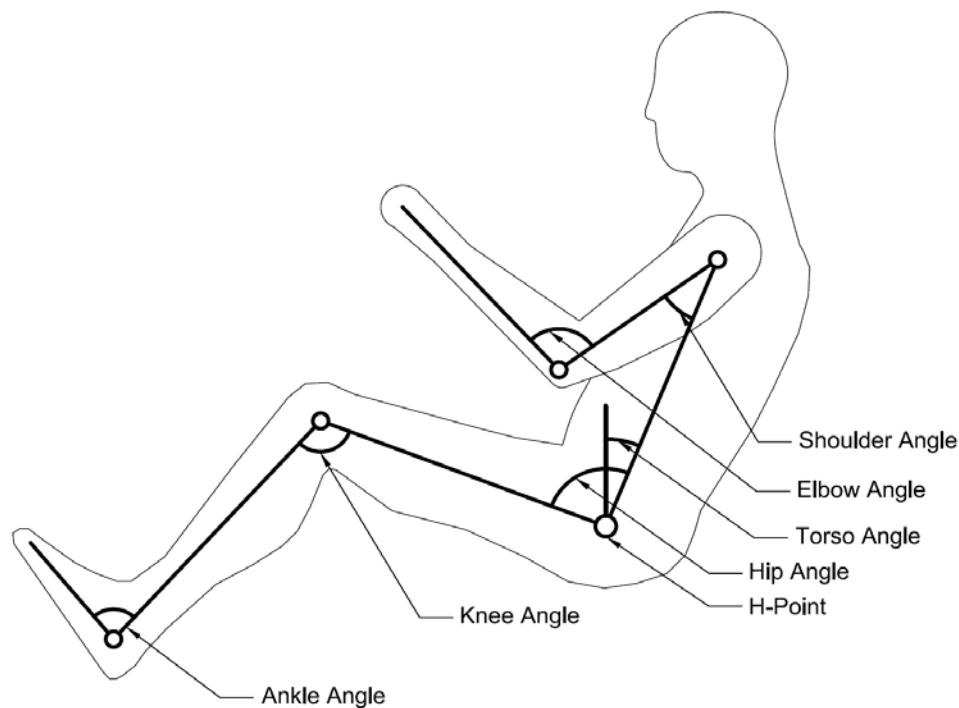


**Figure 3.4** Posture angles as defined in (Kyung and Nussbaum, 2009)

The H-point of the dummy was determined to be  $X= -2280$ ,  $Y= 400$ ,  $Z= 853$  with respect to the origin of the global coordinate system. The angles of the dummy's arms and elbows were not stated in the report. Initially, it was assumed to 0 deg and 90 deg respectively. These angles were determined later after running multiple simulations to arrive at suitable angles that a typical driver would exhibit. Table 3.1 shows the angles used in the validation process

(Baseline Angles). Figure 3.4 shows the location of the H-point along with the relevant posture angle landmarks. The neck and wrist angles were not included in this study.

Table 3.1 contains the maximum and minimum values of posture angles taken from literature. The upper limits are angles a younger driver would exhibit while the lower limits are angles an older driver would undertake. The idea of the experiment is to run multiple simulations where each simulation undergoes either an increase or decrease at a specific joint. This will determine the main effects of posture changes on the injury criteria. Instead of increasing the base angle to the maximum, which isn't possible due to limitation of compartment space, a 10% difference was considered. The following equations illustrate how the angles were computed:

$$Contracted = Base - \frac{|(Min - Base)|}{10} \quad (3.1)$$

$$Extended = Base + \frac{|(Max - Base)|}{10} \quad (3.2)$$

**Table 3.1** Bodily Joint Angles Used for Simulations

<b>Body Joint</b>	<b>Baseline Angle</b>	<b>Min. Angle</b>	<b>Max. Angle</b>	<b>-10% (Contracted)</b>	<b>+10% (Extended)</b>
<b>Left Shoulder</b>	20	0	61	18.0	24.1
<b>Right Shoulder</b>	20	1	67	18.1	24.7
<b>Left Elbow</b>	90	78	174	88.8	98.4
<b>Right Elbow</b>	90	83	169	89.3	97.9
<b>Torso</b>	19	14	45	18.5	21.6
<b>Hip</b>	86	81	137	85.0	91.1

<b>Right Knee</b>	121	93	151	118.2	124
<b>Left Knee</b>	121	94	145	118.3	123.4
<b>Right Ankle</b>	90	70	122	88.0	93.2
<b>Left Ankle</b>	90	84	131	89.4	94.1

### 3.3 THUMS

The Total Human Model for Safety (THUMS) is a human finite element representation developed by Toyota Motor Corporation. It comes in two postures; sitting position which represents a vehicle occupant and a standing position which represents a pedestrian. It comes in three different statures; 50<sup>th</sup> percentile male, 95<sup>th</sup> percentile male, and 5<sup>th</sup> percentile female. The model was created from scanned geometric data of a 39-year-old male with a height of 173 cm and a weight of 77.3 kg with a BMI of 25.8. Figure 3.5 shows the THUMS with and without flesh.



**Figure 3.5** THUMS with Flesh (Left) and without Flesh (R)

The model consists of 204 beam, 395,000 shell, and 1,325,820 solid elements. The major bones, thick ligaments, flesh, muscles, and internal organs were modeled using solid elements. Thin tissues such as cortical bones (thickness <1mm), thin ligaments, membrane tissues were modeled with shell elements. Each element length is approximately 3 to 5 mm. The bones are modeled to have elastic-plastic properties while the soft tissues are modeled to have hyperelastic properties where the stress-strain curve is highly non-linear. In the head portion, the skull and bony parts are modeled using solid elements. The brain consists of white and gray matter.

The cortical bones with thickness less than 1 mm in the torso are modeled with shell elements. The trabecular bones are modeled with solid elements. The skeletal parts of the torso are clavicle, scapula, ribs, pelvis, and spine. The spine consists of many intervertebral discs and a sacrum at the end of the spine. All parts are modeled as deformable. Thick muscles are modeled with solid elements while thin muscles are modeled using spring elements. The soft tissues in the torso are muscles covering the torso. The solid soft tissues such as muscles are model as hyperelastic while the hollow organs are modeled as foam. For the limbs, the cortical and trabecular bones are all modeled using solid elements. The flesh is similar to those in the torso, the muscles are modeled with solid elements. All joints are modeled as bone to bone connections with ligaments. The knee joints are covered by membrane elements representing the capsule. The ankle joint along with other joint types are encased in membrane elements.

The THUMS is suitable for the development of an aged human model through the modification of material properties, compositional, and morphological changes. The effects of aging are simple. The human body deteriorates as we age. The bones continue to strengthen since birth and plateau at the age of 35, and begin to decrease from that point onwards (Frost, 1997). The cortical bone toughness begins to deteriorate a total of 40% by the age of 100 from

40 years of age. The toughness is characterized using a variable known as fracture toughness ( $K_c$ ) (Nalla et al., 2004). The cortical bones' moduli of elasticity ( $E$ ) decrease by 2.3% per decade from its highest value of 15.2 GPa, the strength (yield stress) decreases 3.7% from its highest value of 170 MPa, and  $K_c$  decreases 4.1% from the highest value of 6.4 MPa (Zioupos and Currey, 1998). The tensile properties of cortical bones indicate that the ultimate stress decreases 5%, and ultimate strain decreases 9% (McCalden, 1993). Linear aging functions have been developed to show the decrease in ultimate tensile stress of cortical bones based on age. Among the different researchers' data, large variations exist among them (El-Jawahri, 2010). In the lower regions of the body, the stress in the post-yield portion and failure strains of the elderly is 20% and 10% less than that of young adults respectively (Yamada, 1970). The material properties changes are completed through the material cards in the LS-PrePost. It is done for both flesh and bone parts.

In terms of compositional changes, the cross-sectional area of the ribs decrease approximately  $0.19 \text{ mm}^2$  per year after the age of 25 due to a process known as circumendosteal resorption (Stein, 1976). The compositional changes are completed through manually changing the thicknesses of the cortical bones. Finally, the morphological change is done to the thorax by placing a force on the bottom of the sternum with the spine fixed in place while rotating the rib cage until the 9<sup>th</sup> has been rotated approximately  $7^\circ$  degrees to achieve the "kyphosis" effect (Kent et al., 2005b). This was achieved through a few iterations of running THUMS model only with a force on the sternum until the desired degree was achieved. Then the results (figure 3.6) for the reference geometry of the THUMS model was used for future "Thoracic Change".

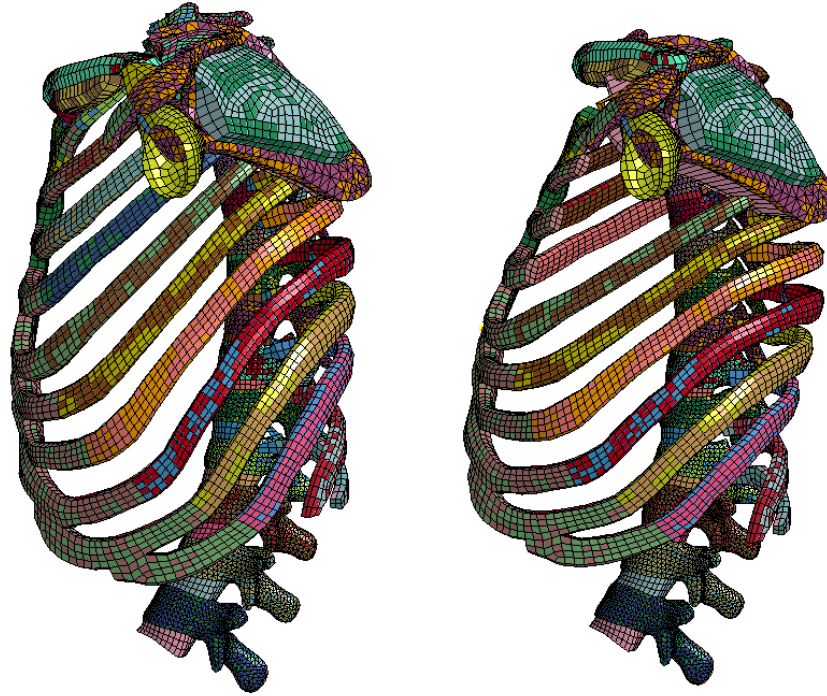


**Figure 3.6** Unmodified Rib Cage (Right) and “Kyphosis” Effect (Left)

The simulations for the THUMS model followed the same procedure as the Hybrid III dummy model. The same vehicle, 2002 Ford Explorer was used. The only exception was the presence of a steering wheel and airbag as shown in figure 3.7. The same seatbelt properties were used along with the same impact velocity. The baseline simulation will be compared to the FMVS208 Report. Subsequently, various simulation of aging factors and their combinations were made to see the effects of an aging driver. The THUMS model with decreased material properties will be known as “old”. The model with decreased bone compositional thickness will be known as “thin”. The model with the “kyphosis” effect will be known as “up”. The following combinations: “old and thin”, “old and up”, and “old, thin, and up” will be assessed. The fully aged driver is the “old, thin, and up” THUMS model.



**Figure 3.7** THUMS Simulation Setup with Steering Wheel and Airbag

### 3.4 Physical Experiments

#### *3.4.1 Simplified Anthropomorphic Test Dummy (ATD)*

To simulate the response of human body during the vehicle crash, a simplified physical anthropomorphic test devices (ATD) was built up. The design of this ATD was inspired by the commercially available crash test dummy model product, ECE-R16 Manikin (formerly known as TNO-10). The ECE-R16 model was developed to test vehicle seatbelt in crash simulations.

Written permission of referring to this specific model for the current work was obtained. This ECE-R16 model was chosen as the prototype because of its relatively low complexity and more practicality than other commercially available ATD models e.g., the Hybrid III and THUMS in terms of design and manufacturing. The testing ATD for this research has the major parts and

joints of a human body with the exception of the arms. The testing ATD consists of head, neck, torso, upper legs, lower legs and feet. These parts are connected together by joints which allow rotational movement about specific axes. To make the testing ATD have a similar weight of a 50th percentile male adult, cast iron blocks are attached to the spine and thighs of the testing ATD as weight blocks. These weight blocks are allocated in such way that the CG coordinates of the testing ATD is corresponding to the CG coordinates specified in the ECE-R16 user manual. The total weight of the testing ATD is about 151 lbs.

The testing ATD was first designed in Solidworks (SOLIDWORKS Corp., 2014) and then the design as shown in figure 3.8 was handed over to the machine shop, one of the auxiliary facilities of College of Engineering, to be fabricated.

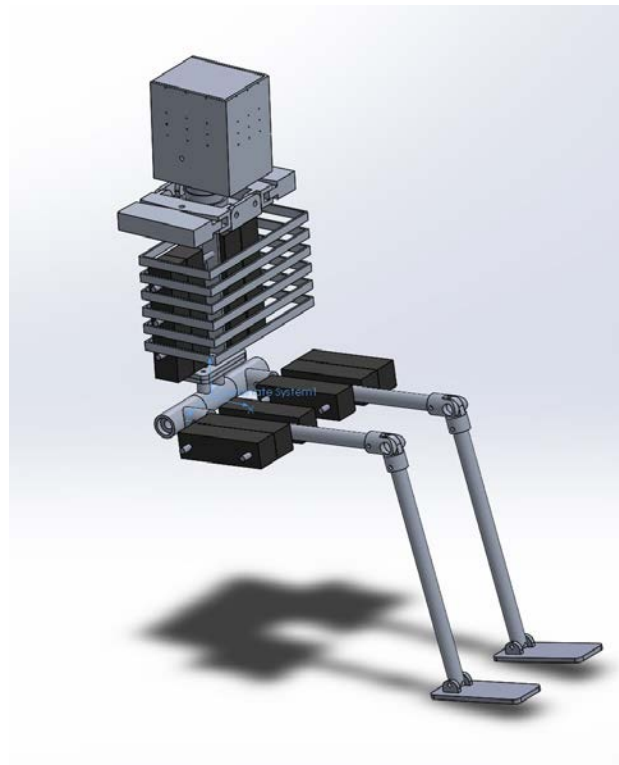


**Figure 3.8.** Schematic of simplified ATD

Considering that the geometry of the head is not strictly related variable to the present work, the head of ATD was simplified to be a hollow aluminum box. There is a sheet fixed in the

middle of the box which serves as a bed plate for the accelerometer. A 3-axial accelerometer was installed at the center of gravity of the ATD's head to measure the acceleration experienced by the testing ATD's head during the impact.

The neck of the ATD model consists of 6 aluminum/rubber discs tightening by a roller chain and a chain tensioner. The rubber discs allow the neck to be able to sustain bending, extension or contraction while the aluminum discs keep some stiffness. A roller chain going through these discs tightens these discs together with a chain tensioner. The neck is connected to the head through the top disc by a shaft and is connected to the spine through the bottom block by bolted connection. Schematic of neck could be seen in Figure 3.9. The dimension and materials of neck discs are listed in table 3.2.

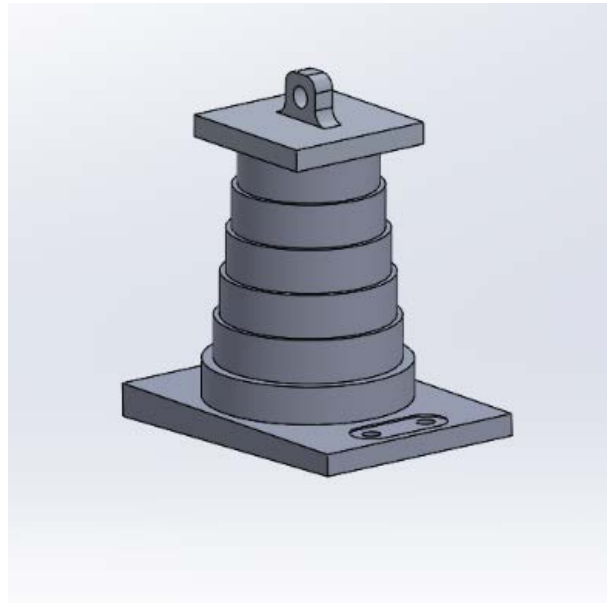


**Figure 3.9** Neck configuration including top disc and bottom block

**Table 3.2** Dimension and material properties of neck discs

Reference No.	Name	Material	Dimensions	Remarks
1	Neck disc-		OD: 2.4"	

	1	Aluminum/ Polyurethane / Neoprene Rubber	ID: 1.2''	Durometer for polyurethane is 40 OO(ultra-soft), durometer for neoprene rubber is 30A (soft)
2	Neck disc- 2		OD: 2.6'' ID: 1.4''	
3	Neck disc- 3		OD: 2.8 ID: 1.6	
4	Neck disc- 4		OD: 3.0 ID: 1.8	
5	Neck disc- 5		OD: 3.2 ID: 2.0	
6	Neck disc- 6		OD: 3.6 ID: 2.4	

The torso of the testing ATD is consisted of a rigid spine, a pair of shoulders and the ribs, see figure 3.10. The material for these three parts is aluminum, taking the advantage of the high strength to weight ratio. A piece of U-channel and two pieces of sheets are welded together to form the spine. On the top of the upper deck sits the bottom block of the neck. The lower deck connects the spine to the hip joint. Ribs are made of aluminum strips, and are installed to the spine by bolted connection. The whole rib cage and the shoulders offer the necessary geometry for the seatbelt to conform and restrain the ATD body.

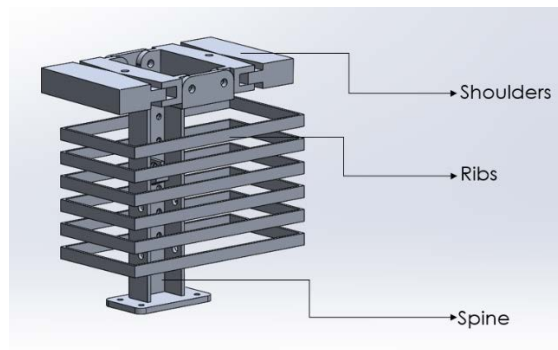


**Figure 3.10** Configuration of torso

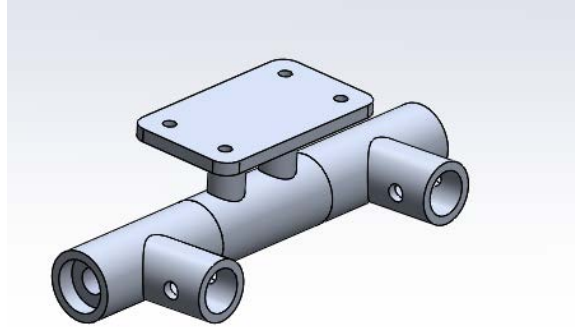


**Figure 3.11** Configuration of hip joint

The hip joint is the part that connects the upper body and lower body. It allows the upper body and lower body to rotate around a specific axis, figure 3.11. Both the upper body and lower body connection are bolted. The testing ATD has upper legs and lower legs and feet, figure 3.12. The upper legs are bolted to the slots welded on the hip-joint at their upper ends while the lower ends are bolted to the knee joints. The knee joints allow upper legs and lower legs to rotate about the horizontal axis separately. Two pieces of rubber tubes are put inside the knee joint, and bolts are placed through the tubes. This mechanism works such that when the bolts are fastened, the nuts and washers will compress the rubber tube in the radial direction, i.e., against the inner surface of the knee joint, which increases the friction between the external surface of the rubber tube and internal surface of the knee joint. Therefore, the angle between upper leg and lower leg can be adjusted to a desired value.



**Figure 3.12** Configuration of lower extremities

The upper legs were bolted to the slots welded on the hip-joint at their upper ends and they were bolted to the knee joints at their lower ends. The knee joints allowed upper legs and lower legs to rotate about the horizontal axis separately. Two pieces of hard rubber tubes were put inside the knee joint, and bolts were placed through the tubes. The outer surface of the rubber tube and inner surface of the knee joints have been roughened to increase friction between surfaces. This mechanism worked such that when the bolts were fastened, the nuts and washers would compress the rubber tubes in the radial direction, i.e., against the inner surface of the knee joint, which increased the friction between the external surface of the rubber tube and internal surface of the knee joint. Therefore, the angle between the upper leg and the lower leg could be fixed at a desired value. When adjustment was needed, loosening the bolts could reduce the friction and let the upper and lower legs rotate freely. Due to the relative hardness of two types of materials, abrasion mostly happened on rubber tube rather than the aluminum. Replaceable rubber tubes could help to keep the knee joints working as expected.

To make the ATD have a similar weight of a 50<sup>th</sup> percentile male adult, cast iron blocks were attached to the spine and thighs of the ATD as weight blocks. The total weight of the ATD was about 151 lbs. The weight blocks on the ATD were allocated in such a way that the center of gravity coordinates of the ATD was mostly close to the CG coordinates specified in the ECE-R16 user manual. The center of gravity of coordinates are presented in figure 3.13.

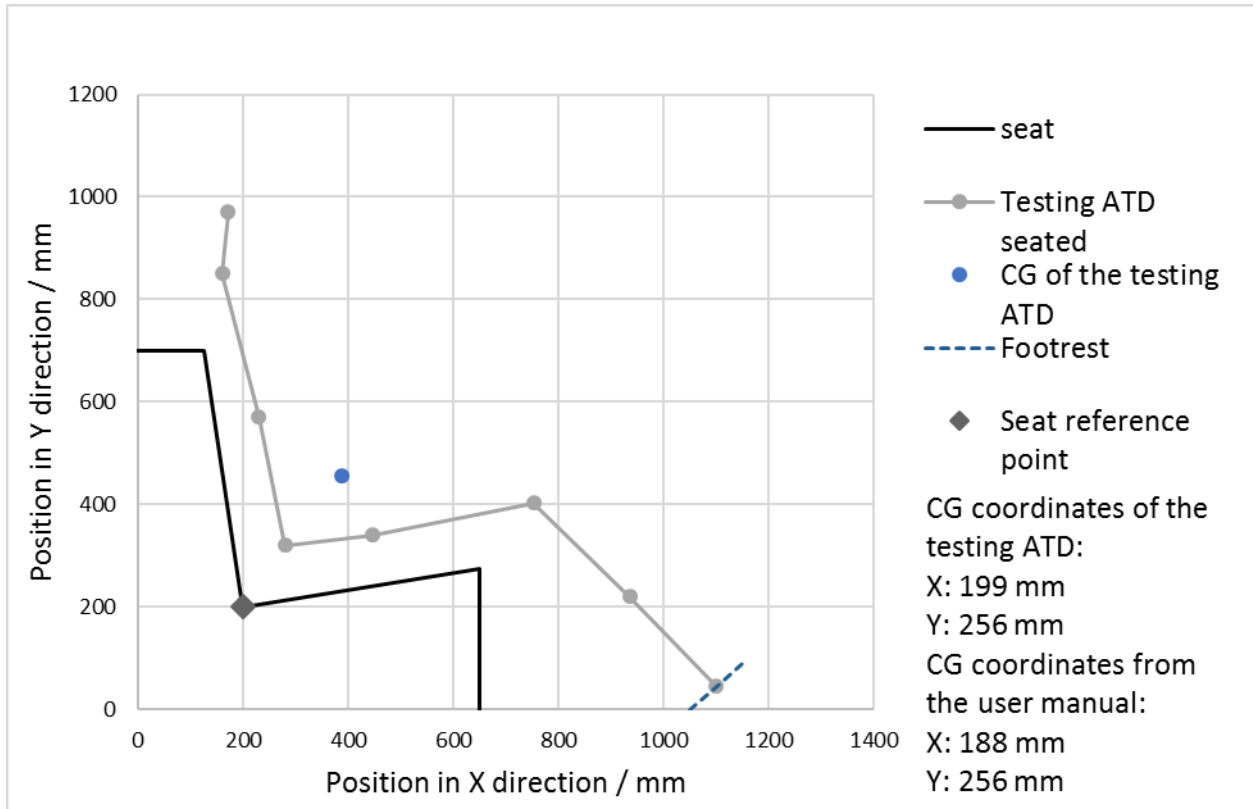


**Figure 3.13** Configuration of lower extremities

### 3.4.2 Sled

The sled test device comprises of two parts, the sled rig (figure 3.14) and the impact pendulum (figure 3.15). The sled rig, which simulates the driving compartment of a vehicle, accommodates the seat and the seatbelt restrain system. The whole sled rig is made of steel tubes welded together. It is designed and built such that it can withstand the impact of the pendulum

many times. The overall dimension of the sled rig is 72 feet (length) \* 30 feet (width) \* 79 feet (height).

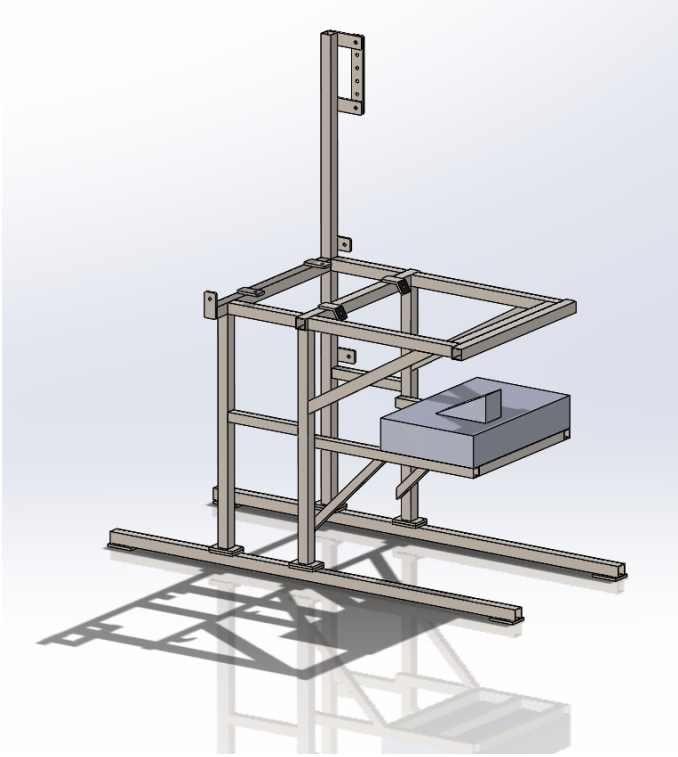


**Figure 3.14** Main structure of sled rig

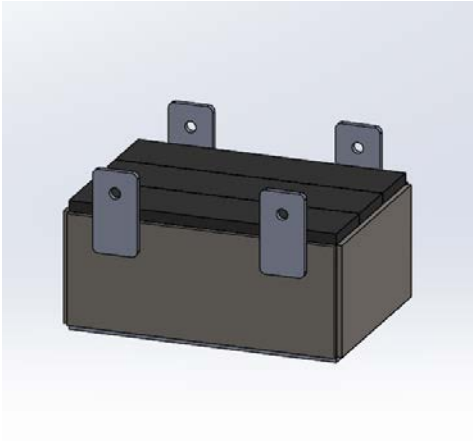


**Figure 3.15** Schematic of impact pendulum

The sled rig is fitted with a vehicle seat and seatbelt taken from an actual vehicle as shown in figure 3.16. The seatbelt anchor is made to be adjustable. It also has an angled foot rest to simulate the gas pedal for the right foot. Rollers are installed for ease of moving the sled; they can be removed easily for the experiment.



**Figure 3.16** Simplified dummy and sled rig

The seat and seat belts are obtained from local mechanic shop. The seat is bolted to the sled rig through four anchors. Due to the limitation of the manufacturing, the tracks which allows the seat to be adjusted are not included. The back cushion of the seat is functional, it can rotate and hold to a specific angle. A standard three-point seatbelt system is chosen. All the three anchors are bolted to the main structure of the sled rig. The pillar loop anchor can be adjusted vertically where height is one of the testing parameters.

The impact pendulum is consisted of cast iron bars that are housed inside a steel sheet box. It weighs approximately 150±1 lbs. The dimensions are 12 inches in length, 8.25 inches in width and 5.75 inches in height. This impact pendulum is designed to be accelerated by gravity. During the tests, the impact pendulum will be lifted by a crane to 45 inches high, inclined manually, and released to swing to provide the impact pulse.

The peak pre-impact velocity of the impact pendulum is computed by calculating the conversion of potential energy at its inclined position and kinetic energy at its pre-impact position, i.e., at the bottom at its swing ( $\Delta h = 0.2\text{m}$ ). The amount of energy that has been consumed in terms of heat and sound is assumed to be insignificant and negligible. The formulas are as follow:

$$mgh = \frac{1}{2}mv^2 \quad (3.3)$$

$$v = \sqrt{2gh} = 1.98\text{m/s} = 4.43\text{mph} \quad (3.4)$$

where m is the mass of the impact pendulum;

g is the gravity constant;

h is the height of the pendulum;

v is the pre-impact velocity.

Currently, there are two widely acceptable configurations regarding the frontal crash test. The first one is developed by the agency NHTSA based on FMVSS 208. The testing protocol is utilized in the New Car Assessment Program (NCAP) in which the testing vehicle crashes at a speed of 30 mph into a rigid barrier that covers the full width of the vehicle. The other one is developed by the Insurance Institute of Highway Safety (IIHS), an independent organization

which carries out research, conducts tests and produces ratings for passenger vehicles. The IIHS's frontal crash tests differs from the NCAP's. The IIHS's tests are offset. For the offset tests, 40% (for a moderate overlap frontal crash test) or 25% (for a small overlap frontal crash test) of the front of the testing vehicle is exposed to an impact with a deformable or rigid barrier respectively.

Compared to the full-width tests, a smaller part of the structure of the vehicle has to deal with the crash energy during offset tests. Therefore, it is more challenging for the structure of the vehicle to maintain intact. Whereas in the full-width tests, more part of the structure of the vehicle is taking part into crumple resulting in less crush in such way that the deceleration that the restraint system has to handle is greater. The offset tests are more demanding of the integrity of the vehicle structure but less demanding of restraint system while the reverse is true in full-width tests (Park et al., 2000). Considering the objective of the present work which is to investigate the effect of driving postures rather than to assess the performance of the structure of the vehicle, a full-width frontal crash testing configuration is considered more suitable.

Furthermore, when the vehicle is crashed into the barrier during the course of the frontal crash test, it experiences three time periods, namely, crushing while moving towards the barrier, being still relative to the barrier and bouncing backwards. For the present work, the sled rig is fixed on the ground, in another word, being still, it could mimic the response of a testing vehicle until the exact moment of bouncing backwards. Another advantage of the fixed sled rig is that it helps to reduce the random error and noise in the acceleration along with time history which are highly likely to occur during a freely movable sled rig configuration.

It should be noted that the current testing speed is far below the testing speed specified in the widely used frontal crash standards. The crash test serves for the purpose of measuring how well a passenger vehicle would protect its occupant during a serious crash accident. The injury of the occupant comes from two adverse effects of an accident, rapid deceleration of the occupant compartment and crush of the occupant compartment survival space. The improving structural design manages to mitigate these two adverse effects. To evaluate the performance of the structure of a vehicle, the test conditions are necessary to be representative of the real world crash environment in which the passenger vehicles are exposed. Thus, the U.S. New Car Assessment Program (NCPA), developed by the NHTSA, employed an impact speed of 35 mph, crashing into a fixed barrier. This test condition could represent the situation of a vehicle moving at 70 mph striking an identical parked vehicle or two identical vehicle moving toward each other at 35 mph (Hershman, 2001). Considering the great kinetic energy carried by the testing vehicle with the impact speed of 35 mph, the testing vehicle is always completely destroyed after the crash.

For the present work, the ideal scenario is to simulate the above-mentioned impact speed but due to limitations, e.g., shortage of funds and tight time schedule of replicating multiple testing apparatus, the impact speed of 35 mph is not practical. That amount of energy may destroy the sled during its initial run. Thus, a lower impact speed was to be adopted.

Nonetheless, we can still investigate effect of different driving postures under the low impact speed. If it is proven that driving posture is one of the parameters that affects the acceleration of the occupant during a crash, then the effect may be greater under a more realistic impact speed. If there is an effect on occupant acceleration under low impact speed, then the

same effect will exist under the realistic higher speed. This can be investigated in the future when a more advanced apparatus and testing setup are available.

### *3.4.3 Instrumentation*

The tests were conducted in the material laboratory of College of Engineering. The sled rig was fixed on ground in an open area of the laboratory. A string was attached to the pendulum. Marks on the string helped ensure for experiment run, the pendulum was lifted to the same height to provide the same peak pre-impact velocity. Rubber dampers were installed in the middle of the extended arms of the sled rig for the point of pendulum impact. It served as reduction of the vibration of the sled rig and lessening the noise in the collected acceleration data for easier data processing. It also served as reduction of possible potential damage to the sled rig.

The ATD was seated on the vehicle seat mounted on the sled rig. The testing ATD was secured by the standard three-point seatbelt system. The testing ATD was adjusted to the required posture in terms of body joint angles before each run of the experiments. Reference lines and coordinate system were marked and created to measure the angles. In order to determine the accelerations of head and torso of the testing ATD, a Summit Instruments 35200B Digital/Analog Accelerometer was mounted both at the center of gravity of head and geometric center of torso. A National Instruments NI cDAQ-9172 data acquisition platform as well as a National Instruments NI-9239 channel to channel isolated analog input module, were utilized to collect the acceleration data. The acceleration data were recorded by the computer program LabVIEW (National Instruments, 2014).

### 3.4.4 Experiment Setup

Driving posture in terms of body joint angles has been selected as the main testing variables to be investigated. Namely, the testing variables are torso joint angle, hip joint angle, left knee angle, right knee angle, left ankle angle, right ankle angle and the height of seatbelt pillar loop anchor. The following figure shows the relevant body joint angles. The neck is not included in the current work.

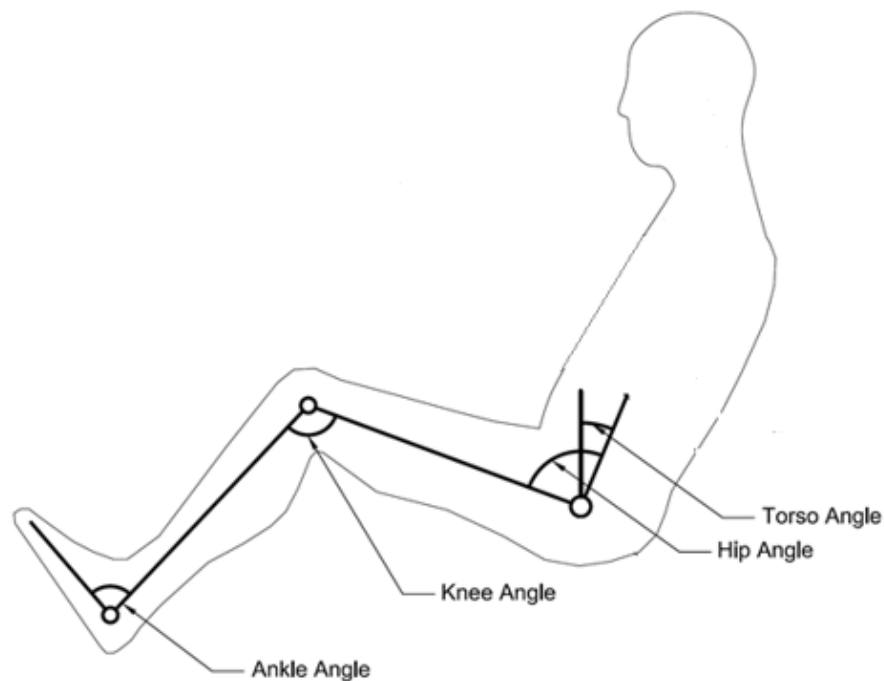


**Figure 3.17** Driving posture angles

If the one-factor-at-a-time experiment design is to be employed, five hundred and twelve runs are needed for the investigation based on seven variables' effect on one response, i.e., head acceleration and chest acceleration. The effect of a factor is defined as the variation in the response which is generated by the change in the level of the factor. Moreover, considering the existence of experimental error, it is desirable to take at least two replications of each run. Then the total amount of experiments would exceed two thousand runs which is too many to be

accomplished within the time schedule of the present work. Thus, a more efficient experiment design is needed.

In general, factorial design is more efficient than the one-factor-at-a-time experiment design where the investigation of multiple factors is involved. It allows the effect of all the possible combinations of the levels of the factors to be investigated within a much less number of experiments. Since there are seven variables to be investigated, and each of them has two levels, namely, smaller or larger body joint angle and lower or higher anchor height the 2K factorial design fits the situation. For the present work, the 2K design requires  $2^7 = 128$  runs, without replication, to investigate the effect of all the seven factors and some of their interactions. Compared to the one-factor-at-a-time experiment design, the higher efficiency of factorial design is obvious.

Considering that the results from finite element simulation indicate that the hip angle, torso angle and both left and right knee angles are mostly likely to have effects on HIC and peak chest acceleration, and to further reduce the amount of experiment that has to be conducted, a  $2^{(7-3)}$  fractional factorial design was employed.

To construct such a design, a basic design which consists of the sixteen runs of for a complete  $2^{(7-3)} = 2^4$  design needs to be completed first. The potential significant factors, torso angle, hip angle, right knee angle and left knee angle are assigned to factors A, B, C and D, respectively. The other three factors, right ankle angle, left ankle angle and seatbelt pillar loop anchor height, would be assigned as factors E, F, and G, respectively. The factor treatment combination is shown as follow:

**Table 3.3** Treatment Combinations

	Basic design				Design generator		
Run	A	B	C	D	E=ABC	F=BCD	G=ACD

1	-	-	-	-	-	-	-
2	+	-	-	-	+	-	+
3	-	+	-	-	+	+	-
4	+	+	-	-	-	+	+
5	-	-	+	-	+	+	+
6	+	-	+	-	-	+	-
7	-	+	+	-	-	-	+
8	+	+	+	-	+	-	-
9	-	-	-	+	-	+	+
10	+	-	-	+	+	+	-
11	-	+	-	+	+	-	+
12	+	+	-	+	-	-	-
13	-	-	+	+	+	-	-
14	+	-	+	+	-	-	+
15	-	+	+	+	-	+	-
16	+	+	+	+	+	+	+

The negative/positive signs indicate low and high level of a specific factor. The signs of basic design follow the rules of complete factorial design, while the signs of the left ankle angle, right ankle angle and seatbelt pillar loop anchor height are generated by the design generator, namely, the products of signs of the corresponding factors.

With such design, only one eighth of the complete  $2^7$  factorial design needs to be conducted, however, the disadvantage is that the effect of higher order interaction, e.g., four-factor interactions, is not detectable. Also, the effect of factors and the effect of their interactions are aliased, complete alias structure of this design is shown in the following table:

**Table 3.4** Alias structure

Aliases			
A=BCE=DEF=CDG=BFG	AB=CE=FG	E=ABC=ADF=BDG=CFG	AF=DE=BG

$B = ACE = CDF = DEG = AFG$	$AC = BE = DG$	$F = BCD = ADE = ABG = CEG$	$AG = CD = BF$
$C = ABE = BDF = ADG = EFG$	$AD = EF = CG$	$G = ACD = BDE = ABF = CEF$	$BD = CF = EG$
$D = BCF = AEF = ACG = BEG$	$AE = BC = DF$	$ABD = CDE = ACF = BEF = BCG = AEG = DFG$	

As can be seen from the table, every main factor is aliased by three-factor interactions. Thus, when we are estimating A, for example, we are really estimating  $A + BCE + DEF + CDG + BFG$ . We assume that the effect comes from the main factor rather than the aliased interaction. This is an application of Ockham's razor, a principle from philosophy that states the simpler explanation is usually better for an occurrence if there are two exist. The corresponding natural values of body joints are summarized from literature (Kyung and Nussbaum, 2009) and presented in the following table:

**Table 3.5** Driving posture angles

Body Joint	Baseline Angle	Low Range	High Range	Low Level	High Level
Torso	19	14	45	15	25
Hip	86	81	137	85	95
Right Knee	121	93	151	100	110
Left Knee	121	94	145	105	115
Right Ankle	90	70	122	85	95
Left Ankle	90	84	131	85	100

Among the angles, as previously mentioned, left and right angles are bilaterally asymmetric (Hanson et al., 2006a).

The idea is to run experiments following the treatment combination. However, it is not possible to set the low and high levels of the body joints to ideal low and high range due to the physical limitation of the simplified ATD. Then Low level and high level values are set mostly possibly close to the low range and high range summarized from literature. For the seatbelt pillar loop anchor height, a vertical height difference between low and high level is 10inch.

### 3.4.5 Data Acquisition and Process

During the execution of the experiment, the impactor is raised, released, and swung freely into the sled rig. The accelerometers installed on the ATD records the acceleration. The accelerometers are mounted in such way that their axes follow the coordinate system convention specified in SAE J211-1(2007): Instrumentation for Impact Test, Part 1, Electronic Instrumentation, see the previous figure 3.15.

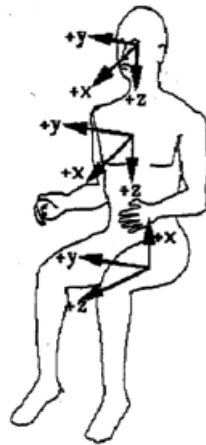


**Figure 3.18** Standardized coordinate systems orientation adapted from (SAE, 2007)

**Table 3.6** Channel Frequency Class Reprinted from (Huang, 2002)

Typical Test Measurement	Channel Class
<u>Vehicle structure acceleration for use in:</u>	
<b>Total Vehicle comparison</b>	<b>60</b>
Collision simulation	60
Component analysis	600
Integration for velocity or displacement	180
<b>Barrier face force</b>	<b>60</b>
<b>Belt restraint system load</b>	<b>60</b>
<u>Occupant:</u>	
<b>Head acceleration</b>	<b>1000</b>
<b>Chest acceleration</b>	<b>180</b>
deflection	180
<b>Pelvis</b>	
acceleration	<b>1000</b>
force	1000
moments	1000
<b>Femur/knee/tibia/ankle</b>	
force	<b>600</b>
moments	600
displacements	180
<b>Sled acceleration</b>	<b>60</b>
<b>Steering column load</b>	<b>600</b>
<b>Headform acceleration</b>	<b>1000</b>

The responses are acquired as raw data. The raw data need to be filtered regarding to the specific Channel Frequency Class prior to further analysis. The Channel Frequency Selection could be seen in the following table:

CFC-1000 and CFC-180 are chosen to filter the raw data of the head acceleration and chest acceleration correspondingly using the following equation:

$$Y[t] = a_0X[t] + a_1X[t - 1] + a_2X[t - 2] + b_1Y[t - 1] + b_2Y[t - 2] \quad (3.3)$$

where  $X_t$  is the input data stream

$Y_t$  is the filtered output data stream

T = the Sample Period in Second

$$w_d = 2 * \text{Pi} * \text{CFC} * 2.0775$$

$$w_\alpha = \sin(w_d * T / 2) / \cos(w_d * T / 2)$$

$$a_0 = w_\alpha^2 / (1.0 + \sqrt{2} * w_\alpha + w_\alpha^2)$$

$$a_1 = 2 * a_0$$

$$a_2 = a_0$$

$$b_1 = -2 * (w_\alpha^2 - 1) / (1 + \sqrt{2} * w_\alpha + w_\alpha^2)$$

$$b_2 = (-1 + \sqrt{2} * w_\alpha - w_\alpha^2) / (1 + \sqrt{2} * w_\alpha + w_\alpha^2).$$

MATLAB (Version R2015a, MathWorks. Inc.,) was employed as an integration tool to calculate  $HIC_{15}$  values after filtering head acceleration data. While peak values were picked from the filtered chest acceleration data. Then the  $HIC_{15}$  and peak chest acceleration are plugged into Minitab (Version 17, MINITAB statistical software. Minitab Release,) to be analyzed using the fractional factorial design analysis function.

### 3.4.6 Experimentation Limitation

Due to the limitation of ATD manufacturing accuracy, the measurement and setting of body joint angles could not be achieved at the accurate level. An error of  $\pm 5$  degree was inevitable. To some extent, this might reduce the reliability of the present work. However, a better ATD model with a fine joint angle control function could improve this problem for the future study. Secondly, more experiments will be beneficial to separate the main factors from

aliased structures. As mentioned above, the main factors and their interactions are aliased together under such experiment design. To give clear estimate of the main factors and their interactions, sequential complementary experiments would be beneficial.

## Chapter 4 Results and Discussion

### 4.1 Driving Posture Changes due to Aging: Frontal Crash Simulation Using FE

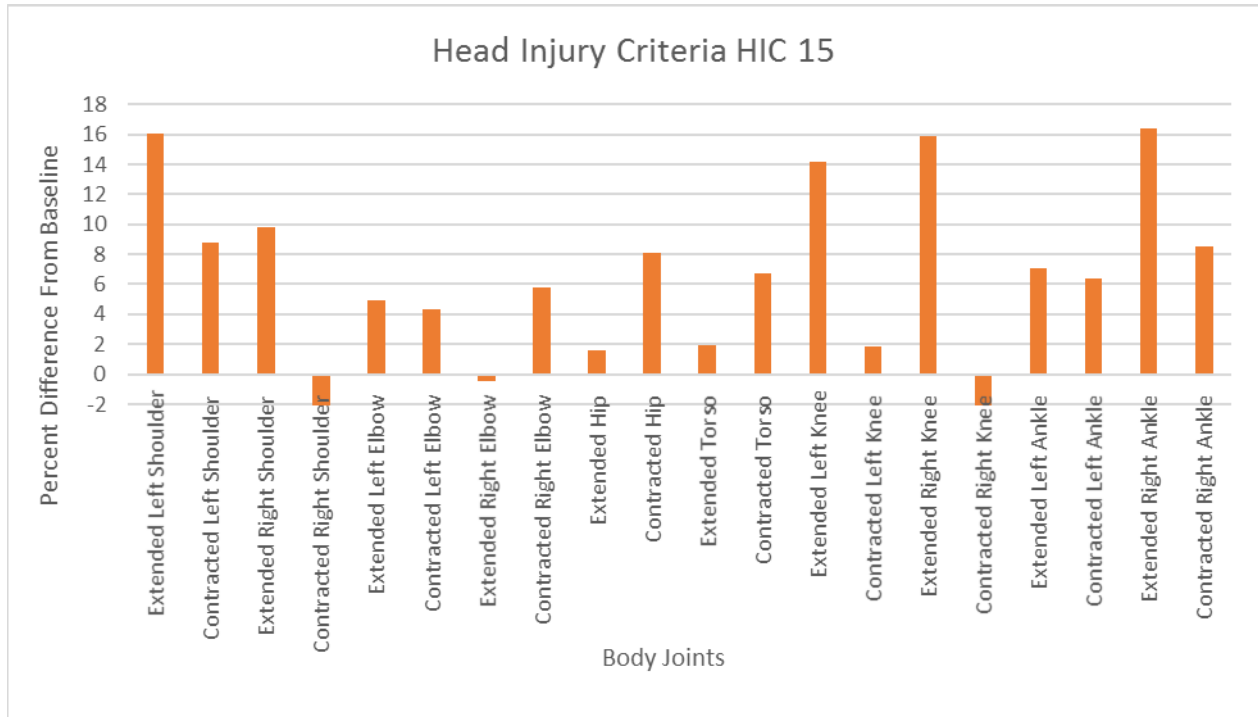


**Figure 4.1** HIC<sub>15</sub> differences

The results are presented in the form of percent differences from the baseline simulation to show the effect of posture change on the outcome. As previously stated, older drivers tend to sit closer to the dash which express contracted joint angles than younger drivers. The overall results in figure 4.1 shows that extended angles exhibit increased HIC values. The left and right elbow joints have minimal influence on the HIC outcome. Whereas, the shoulders do affect the HIC. The extended left and right shoulders yielded 16% and 10% increase respectively. The results are not symmetric because the joint angles are asymmetric as evident in the data taken

from literature. But, the baseline angles are symmetric because they were derived from the FMVSS 208 Ford Explorer physical crash report. During the crash, the shoulders move forward and the arms act as a brace for the torso as contact is made with the vehicle interior as shown in figure 4.2. The head continues to travel forward even after the torso is restrained by the seatbelt. As the body undergoes deformation by the seatbelt and braced arms, the head continues to move forward. The left shoulder yielded a higher value due to the orientation of the shoulder belt.

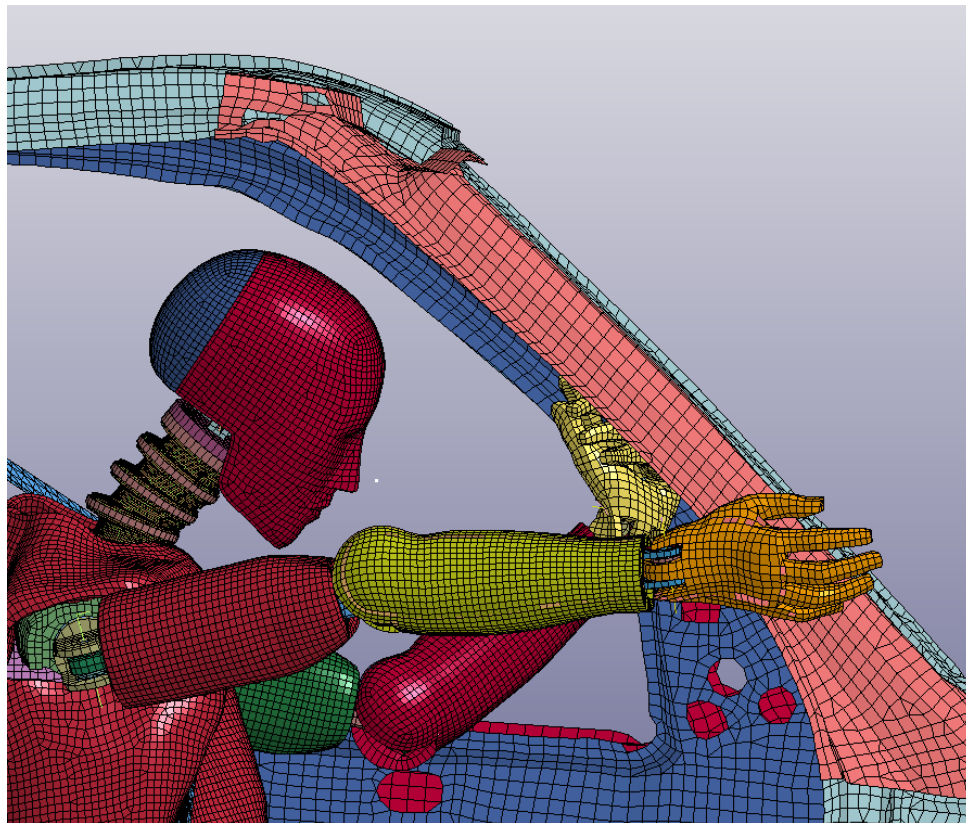


**Figure 4.2** Left arm acting as a brace (extended left shoulder simulation)

Focusing on the knees, the lower extremities affect the HIC. The driver inside the compartment during a crash can be modeled as a parallel system of masses and springs. The head, torso, and lower extremities are masses that are restrained, or going to be restrained by springs. The airbag, seatbelt, and vehicle interior work as springs. In the absence of airbag, while

the torso and extended legs are restrained, the head continues forward. The right ankle affects the HIC as much as the legs whereas the left ankle does not. In table 3.1, the low and high ranges for the right ankle are lower than that of the left ankle. This difference shows that the right foot is used for the accelerator. The heel of the right foot is in contact with the floorboard at an angle, and it acts like a roller support with friction as a resistant force. The incoming force of moving leg, parallel with the leg, is resisted by the friction until it stops completely when contact with the vehicle is made as shown in figure 4.3.

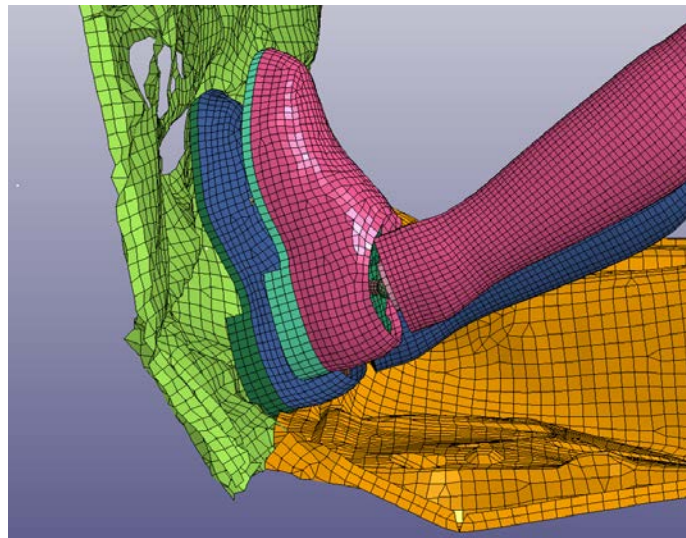


**Figure 4.3** Right foot impacting vehicle interior

As for chest acceleration, the sitting closer to the dash do have implications of higher chest acceleration as shown in figure 4.4. When the driver sits closer to the dash, empty space can exist between the driver's upper back and the seat back as evident in figure 4.5. When the driver is more laid back into the seat, the lower back is firmly supported by the seatback. The contracted torso causes a 7% increase in peak chest acceleration. The curve has a slightly higher slope than the baseline as shown in figure 4.6. As for the other posture changes such as leg and arm joints which are not in direct relation to the seatbelt, 6% or less increase was measured.

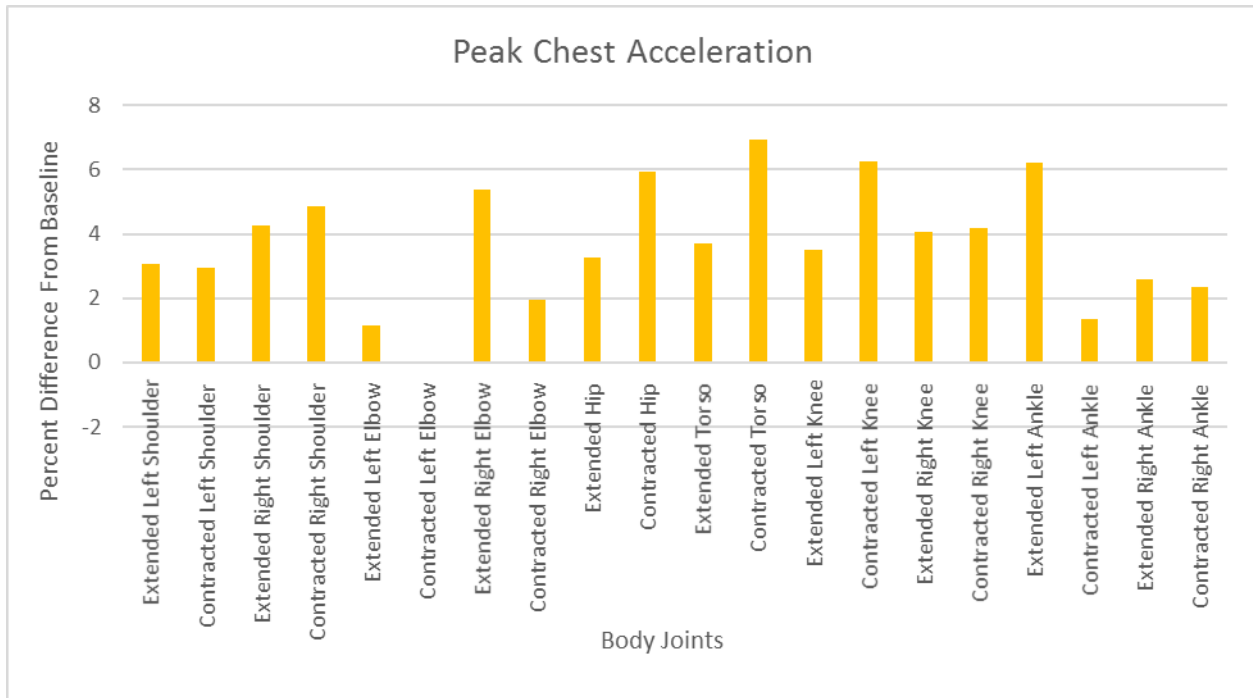


**Figure 4.4** Chest acceleration differences

The chest acceleration is dependent on the seatbelt stiffness and slack (Huang, 2002). The seatbelt’s properties remained the same and the slack was kept to a minimum throughout all the simulations. The chest accelerometer location changes when the torso and hip joints change. The fitting of the seatbelt is dependent on the orientation of the torso. The chest acceleration can be described using a two degree of freedom (dof) dynamic model as shown in figure 4.5. The upper mass is the chest and lower mass is the hip and lower extremities while the head portion is absent for a simplification of the model. The upper and lower springs represent the stiffness of the shoulder and lap belts respectively. Using LaGrange’s Equation to solve for the following equation of motion for chest acceleration.

$$\ddot{\theta} = \frac{-F_1 \cos\theta + F_2 \frac{m_1 + m_2}{m_2}}{L(m_1 + m_2 \sin^2\theta)} \quad (4.1)$$

Where  $F_1$  is the force caused by the impact between vehicle interior and occupant's lower extremities and  $F_2$  is the force caused by the torso and the seat back which creates a moment about the pivot point in the hip. The magnitude of the forces is dependent on the seatback slack and stiffness.

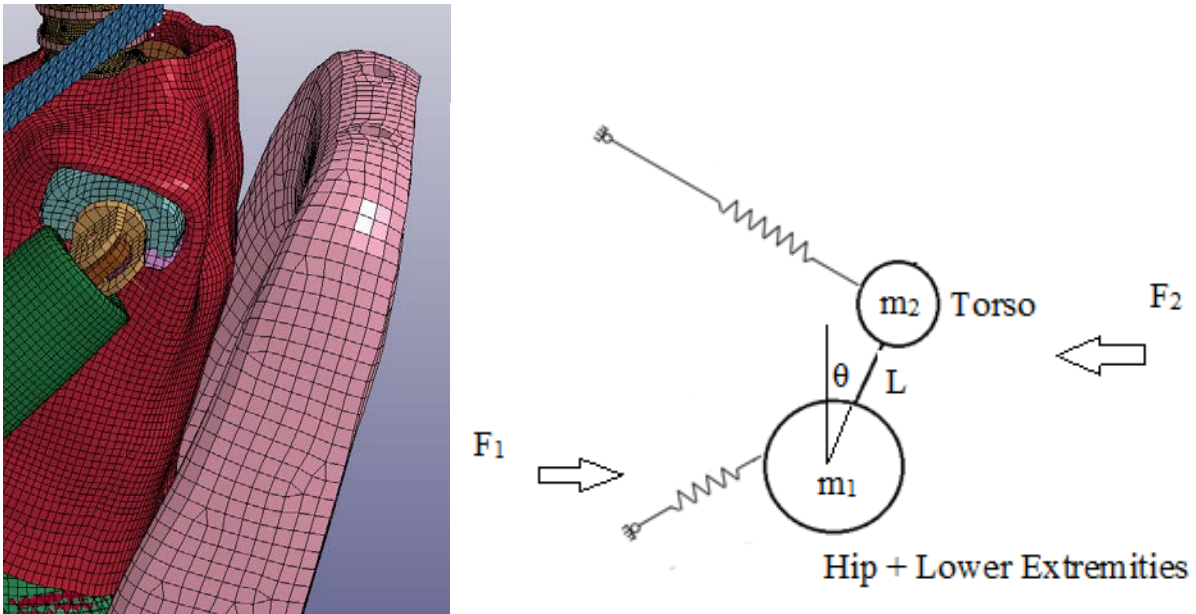


**Figure 4.5** Spacing between driver's back and seat back (L) and 2-dof model (R)

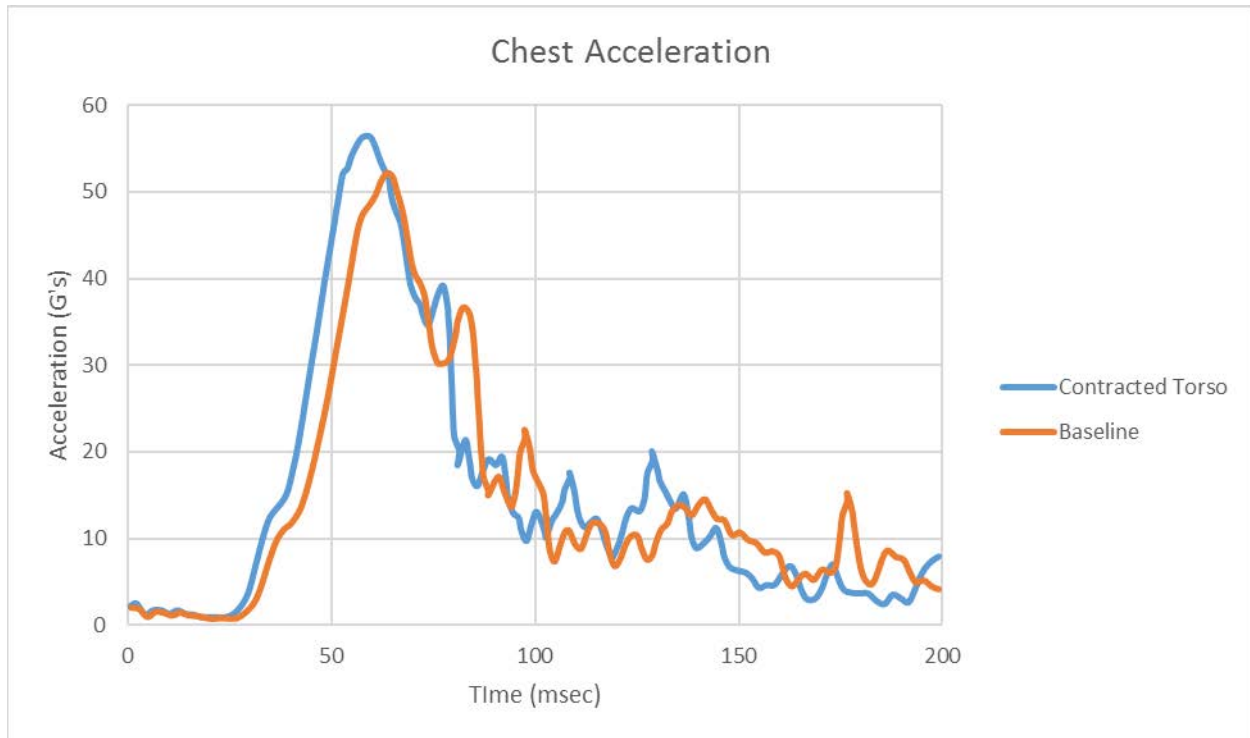


**Figure 4.6** Comparison of chest acceleration between baseline and contracted torso

For the pelvis acceleration, there is disparity among the results as shown in figure 4.7 but overall, all the percent differences are 6% or less which. For the most part, the contracted angles do show slightly decreased values. The randomness may just be an indication of unlikeliness that posture changes affect the pelvis acceleration outcome. Pelvic injury is a likely outcome in side impacts (Melvin et al., 1976). The major causes for injury in the pelvic area is due to the limited crush distance (the door panel), the impacting vehicle penetrating the driver compartment, the likeliness of the driver ejecting from the driver's window to interact with external objects, and the inadequacy of the seatbelt's ability to restrain the driver lateral. As with frontal impact, the hip is least affected by varying posture.

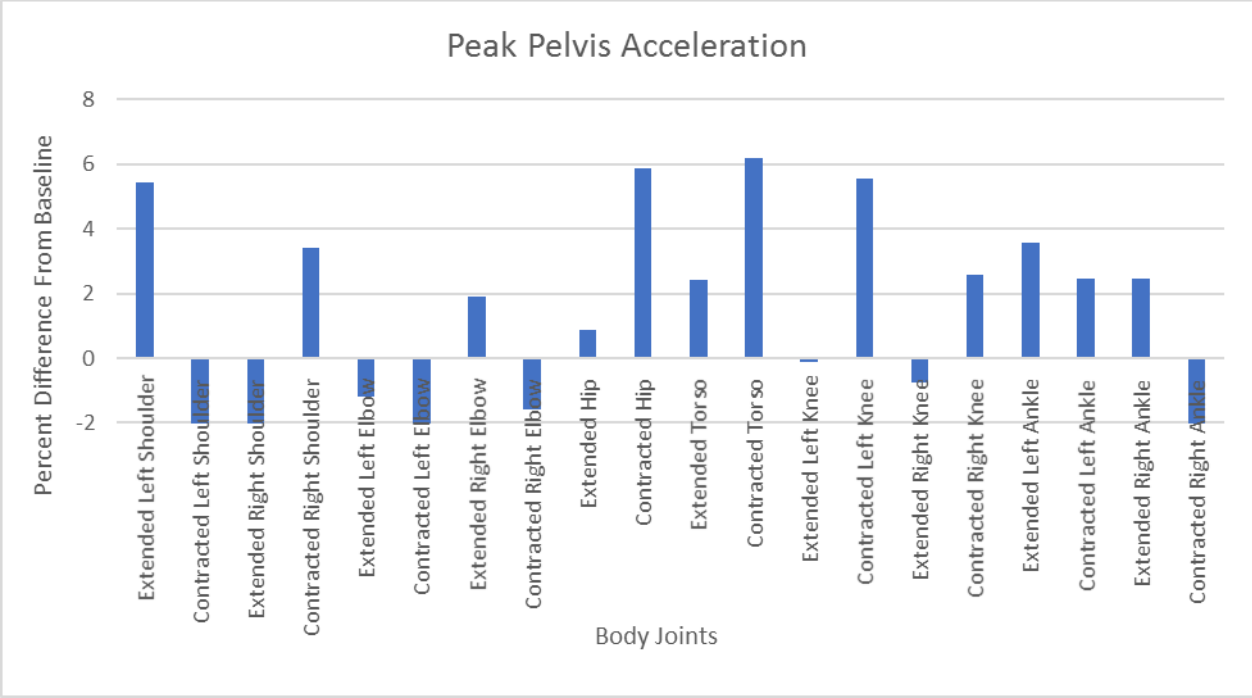


Figure 4.7 Pelvis acceleration differences

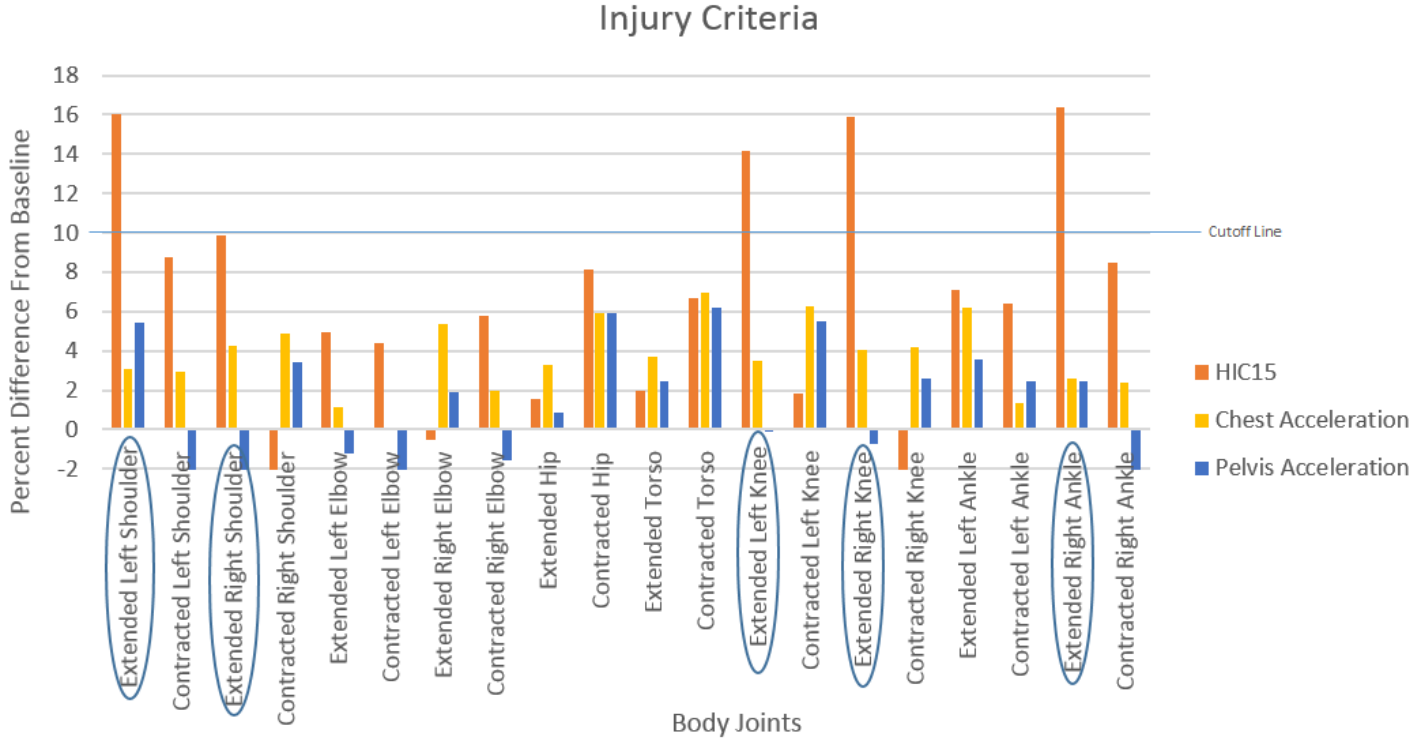
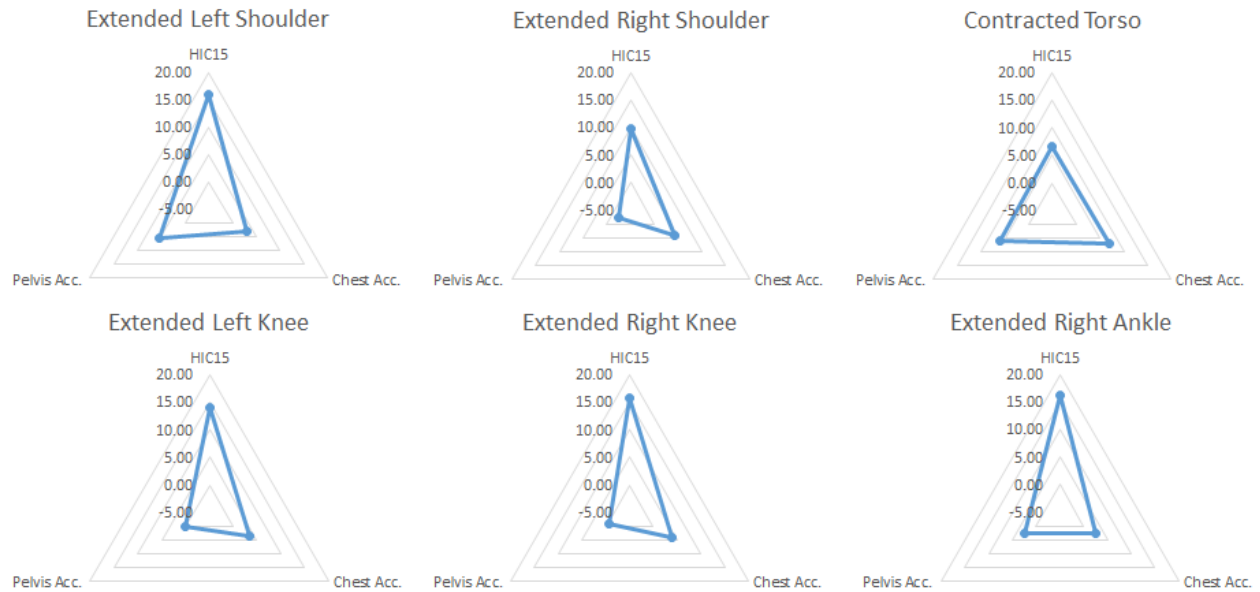


Figure 4.8 Combination of the previous injury criteria charts

To better understand the effect of posture changes, only the relevant postures were collectively investigated. These postures were selected using a cutoff point of 10% difference as shown in figure 4.8. The postures selected are extended left shoulder, extended right shoulder, contracted torso, extended left knee, extended right knee, and extended right ankle. The contracted torso is included because it yielded the higher chest acceleration. To investigate how each joint affects each injury criteria, a triangle radar plot was plotted for each joint where each axis represents an injury criterion as shown in figure 4.9. By extending the left shoulder, the HIC increases 16% while the pelvis and chest acceleration remains mostly unchanged. As for extending the right shoulder, the HIC and chest acceleration increases approximately 10% and 4% respectively while the pelvis acceleration decreases by 2%. When the driver sits closer to the steering wheel, the HIC, chest acceleration, and pelvis acceleration increase approximately 7%. By extending both the left and right knees, the HIC increases approximately 14% and 16% respectively while the chest acceleration increases slightly and pelvis acceleration remains the same. Finally, the extended right ankle which operates the accelerator and brake pedal, increases the HIC approximately 16% while the chest and pelvis acceleration remain largely unchanged.



**Figure 4.9** Triangular plots showing relevant body joints

For the aging aspect of the investigation, the old postures are compared with their young counterparts, thus comparing young and old postures based on the literature review where older drivers tend to sit closer to the wheel (contracted angles) while younger drivers sit further from the wheel (extended angles). Figure 4.10 shows the comparison between the two but it is important to note that these values are normalized by dividing by the baseline values. Therefore, the values that are to be stated in the following are not accurately visualized in the figure. Additional calculations were conducted to come up with the values.

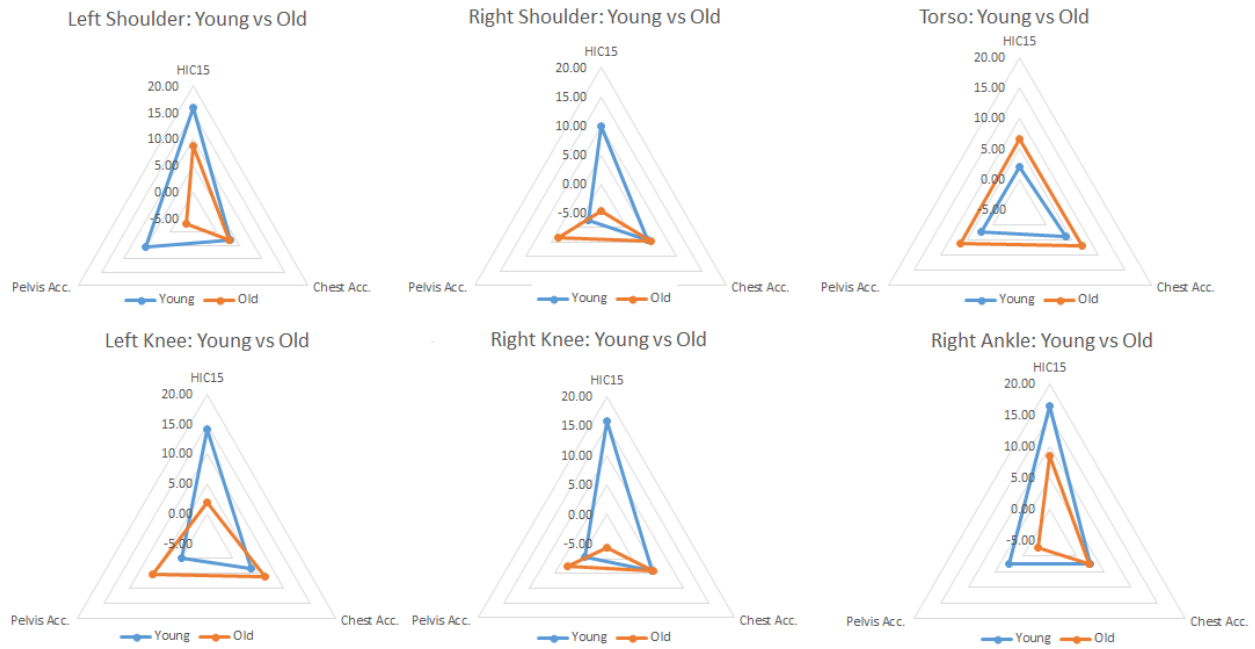


**Figure 4.10** Triangular plots comparing young and old postures

Overall, there are noticeable differences between young and old postures. The young postures generally exhibit higher values for the injury criteria with the exception of the torso. The old torso posture yields approximately 5%, 3%, and 4% higher values than the young torso posture for the HIC, chest acceleration, and pelvis acceleration respectively. Focusing on the chest acceleration, the old left knee and old torso postures are approximately 3% higher. For all others, the values are the same.

As for the pelvis acceleration, the old postures generally show higher values than that of the young postures except for the left shoulder and right ankle. They are higher by 8% and 5% respectively. For the right shoulder, and both left and right knees, the young postures show approximately 6%, 6%, and 3% higher values respectively. The highest differences occur in the HIC. In general, the young postures except the torso yield higher values. The young left and right

shoulders are 6% and 13% higher respectively. The young left and right knees are 11% and 19% higher respectively. For the young right ankle posture, HIC is 7% higher.

#### 4.2 Driving Posture Changes in Frontal Crash due to Aging using Simplified ATD

The FE simulations show that driving posture does not have an effect on the pelvis acceleration because the location of the H-point during pre-impact remains unchanged.

Therefore, only HIC<sub>15</sub> and chest acceleration will be investigated.

##### *4.2.1 Head Injury Criteria*

*HIC<sub>15</sub>* values from 16 runs of experiments are summarized in the following table:

**Table 4.1** HIC<sub>15</sub> values

Treatment	<i>HIC<sub>15</sub></i>	
	Replication_1(g)	Replication_2(g)
1	127.95	145.72
2	201.59	192.61
3	72.66	39.11
4	131.09	120.83
5	36.42	50.09
6	138.11	78.35
7	136.04	168.46
8	64.65	87.10
9	33.63	35.21
10	315.72	318.15
11	126.32	128.20
12	215.47	175.31
13	377.43	359.20
14	326.68	347.04
15	67.57	90.98
16	124.12	116.87

After the acquisition of the *HIC<sub>15</sub>* values, factorial analysis was conducted using Minitab. Figure 4.1 shows the working environment of Minitab, with the data plugged in. As previously mentioned, the main factors, torso angle, hip angle, left knee angle, right knee angle, left ankle angle, right ankle angle and seatbelt pillar loop anchor height are coded as A, B, C, D, E, F and G, and their interactions are represented using the product of coded names, e.g., the interaction of torso angle and hip angle are coded as AB. For the convenience and conciseness of description, the following wording would use coded names of the interaction of factors.

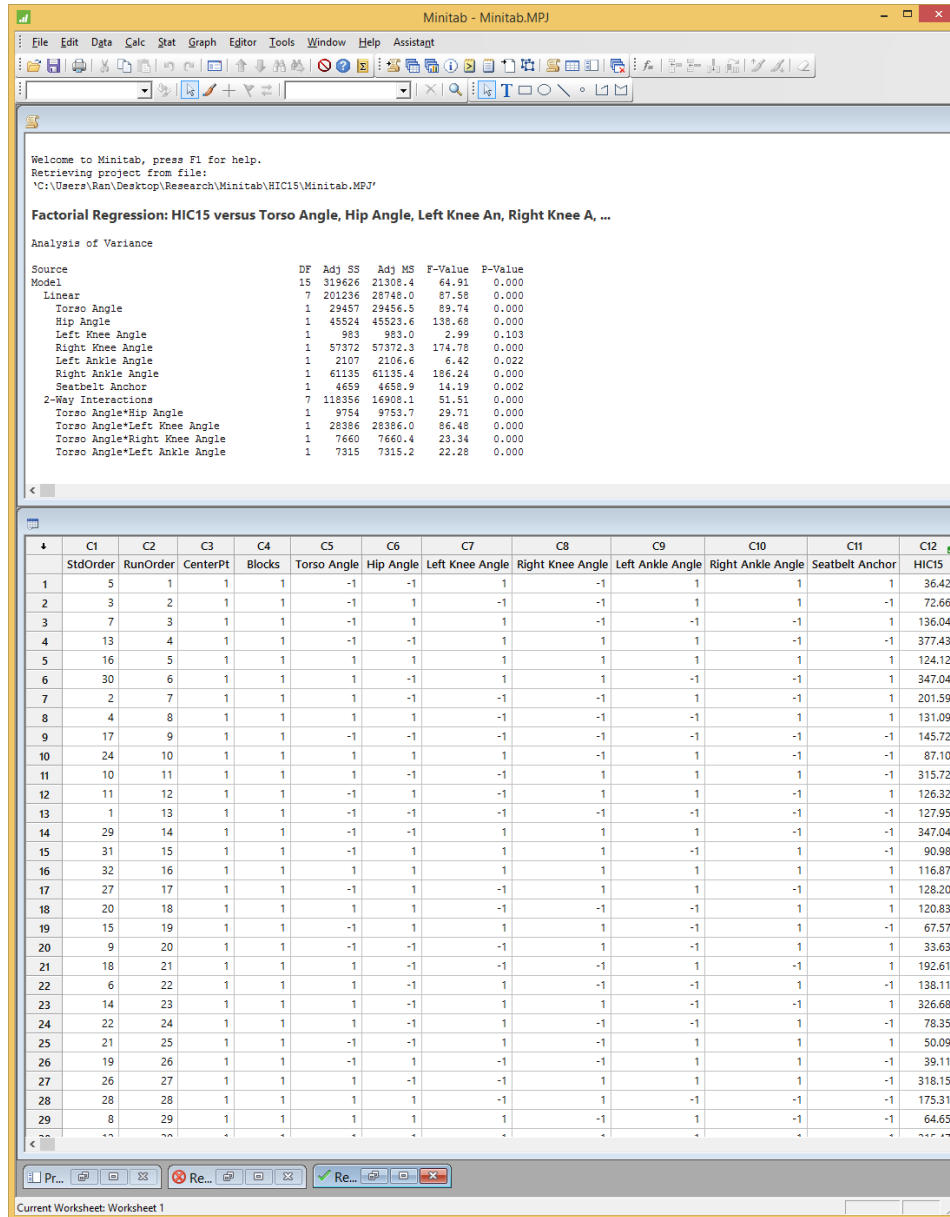


Figure 4.11 Working environment of Minitab

The effects plot of the standardized effects, figure 4.12, shows that for the main factors, left knee angle and left ankle angle do not have significant effect on the response of  $HIC_{15}$ . The torso angle, hip angle, right knee angle, right ankle angle, and seatbelt pillar loop anchor height are significant factors that affect the response of  $HIC_{15}$ . For the low order interactions, it turns

out that AB, AC, AD, AE, AF, AG, BD are significant in terms of effect on response of  $HIC_{15}$ .

The residual plots, figure 4.12, show that the linear regression model is properly fitted.



Figure 4.12 Significant factor plot for  $HIC_{15}$

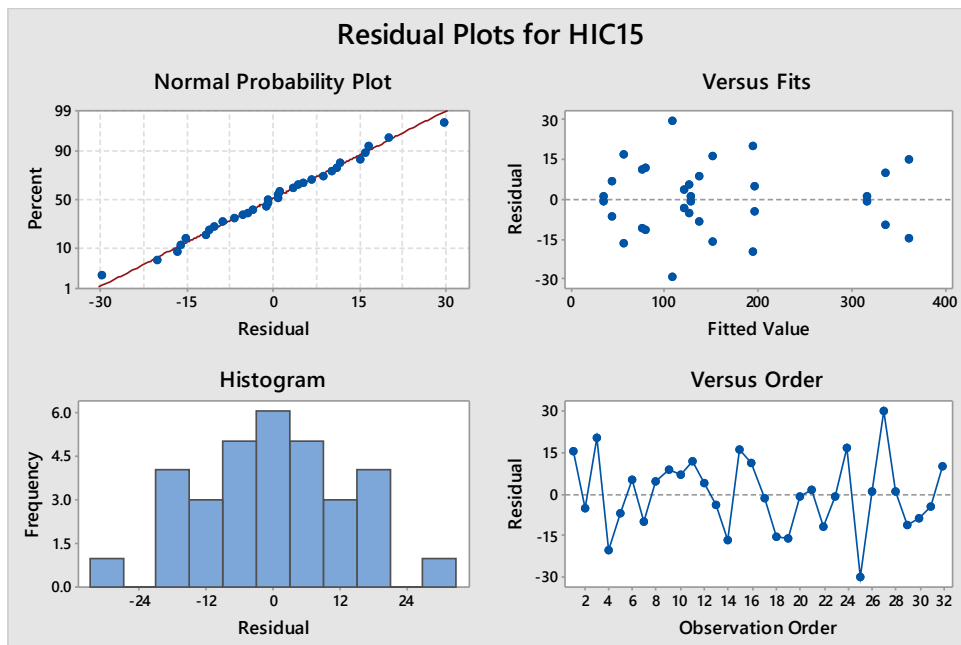


Figure 4.13 Residual plot for  $HIC_{15}$

Except for the screening of significant factors, the data analysis establishes a linear regression model of HIC<sub>15</sub> response. The residual plots, figure 4.13, show that the linear regression model is properly fitted. The formula of the linear regression model is presented as following:

$$\begin{aligned}
 \text{HIC}_{15} = & 154.65 + 29.96 \text{ Torso Angle} - 38.10 \text{ Hip Angle} + 5.92 \text{ Left Knee Angle} \\
 & + 42.72 \text{ Right Knee Angle} + 8.49 \text{ Left Ankle Angle} - 44.09 \text{ Right Ankle Angle} \\
 & - 12.45 \text{ Seatbelt Anchor} - 17.08 \text{ Torso Angle*Hip Angle} \\
 & - 30.16 \text{ Torso Angle*Left Knee Angle} + 15.09 \text{ Torso Angle*Right Knee Angle} \\
 & - 15.50 \text{ Torso Angle*Left Ankle Angle} + 27.39 \text{ Torso Angle*Right Ankle Angle} \\
 & + 22.94 \text{ Torso Angle*Seatbelt Anchor} - 28.67 \text{ Hip Angle*Right Knee Angle} \\
 & - 0.64 \text{ Torso Angle*Hip Angle*Right Knee Angle}
 \end{aligned}$$

The estimation of the effect of a single factor could be established based on this linear regression model. The idea is to plug in high and low level ( $\pm 1$ ) of a specific factor into this model and then use linear interpolation to analyze. For example, for the factor of torso angle, the high and low level yield HIC<sub>15</sub> values of 190.13 and 136.85 respectively. Linear interpolation shows that for one degree increase in torso angle, the HIC<sub>15</sub> value has a 3.16% growth correspondingly. Another example is the right ankle angle, numeric analysis shows that for each degree increase the response has a 27.99 decrease. However, such estimation only applies between high and low levels mentioned above in table 4. Due to fabrication issue and instrumentation limitation, experiment involving factors that are out of high and low level

domain is not conducted. Whether the present linear regression model applies in a wider range and if there is a more suitable model to estimate such effects need future work to verify.

A difference was found between the effect of left side joint angle and right side joint angle. The right knee and right ankle angle have a significant effect on the  $HIC_{15}$  while the effect of the left knee angle and left ankle angle is likely negligible. This could be partly attributed to the different testing angles of the left side body joint and right side body joint. As mentioned previously, bodily joint angles are bilaterally asymmetric. One possibility is the presence of the rigid gas paddle. At the initial condition before the impact occurs, right foot of ATD is resting on the gas paddle, set to a desired angle. During impact, left side of lower extremity of ATD could respond freely to the impact pulse while the motion of right foot is obstructed by the gas paddle. Under such circumstance, the right side of lower extremity acts like a bracing pole which might change the mechanics of the ATD in a way that changes the acceleration experienced by the whole body, especially the head.

Another factor that has a significant effect on  $HIC_{15}$  is the height of the seatbelt pillar loop anchor. As mentioned above, a three-point seatbelt restraint system is employed for the current work, figure 4.14. The end bracket and buckle are mounted on the sled rig and remained fixed while the height of the pillar loop anchor is considered as one of the testing variables. The configuration with a lower pillar loop anchor yielded a higher  $HIC_{15}$  value. A possible explanation is that as the pillar loop anchor height changed, the contact between the seatbelt and ATD alter correspondingly. Lower pillar loop anchor lessens the slack of seatbelt such that the seatbelt has a better restraint on the ATD.

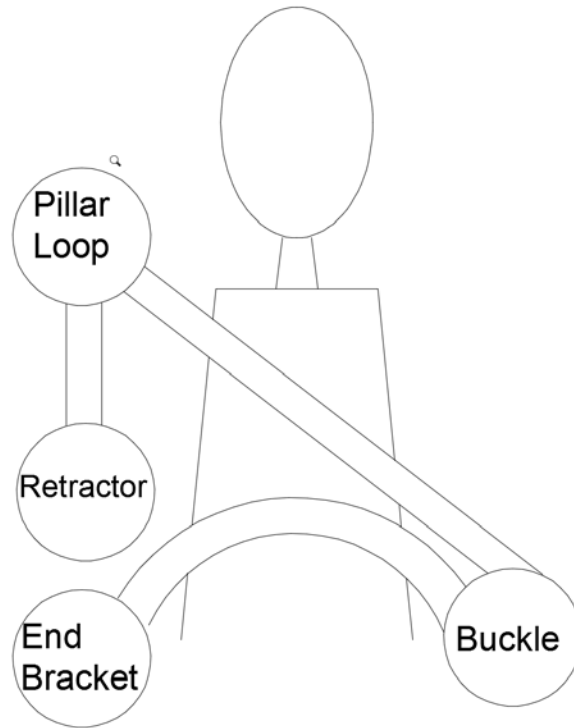


**Figure 4.14** Schematic of a standard three-point seatbelt restraint system

Focusing on the upper body, the torso angle and hip angle both have significant effect on HIC<sub>15</sub> value. Larger torso angle is corresponding to higher HIC<sub>15</sub>.

#### 4.2.2 Peak Chest Acceleration

Peak resultant chest accelerations from 16 runs of experiments are presented table 4.1.

**Table 4.2** Peak resultant chest acceleration

Run (See Table 3.3)	Peak Resultant Chest Acceleration	
	Replication_1(g)	Replication_2(g)
1	4.93	4.71
2	4.87	4.67
3	4.68	4.22
4	4.67	4.63
5	4.26	4.44

6	4.57	4.53
7	3.97	3.96
8	4.15	3.01
9	4.13	4.18
10	5.28	4.79
11	3.88	3.48
12	6.58	6.28
13	4.67	4.95
14	6.31	5.88
15	5.16	5.94
16	4.99	5.38

Similar to HIC<sub>15</sub>, data are analyzed using Minitab. Significant factors that affect peak resultant chest acceleration are presented in the following figure 4.15 and the residuals are plotted in figure 4.16.

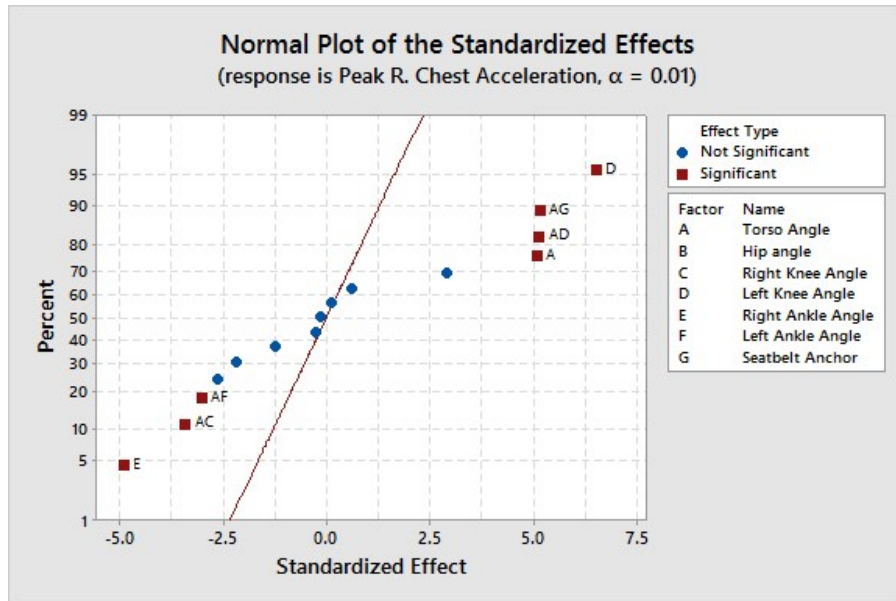


**Figure 4.15** Significant factor plot for peak resultant chest acceleration

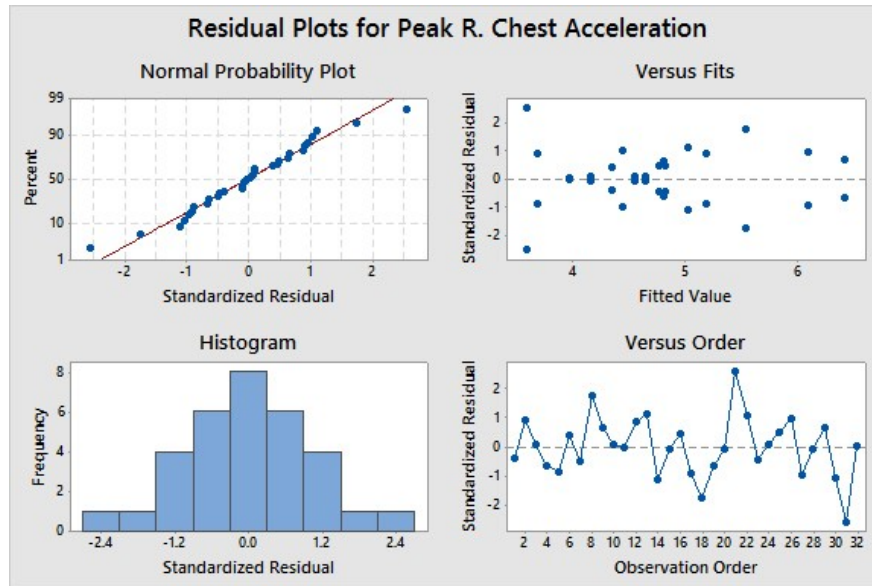


**Figure 4.16** Residual plot for peak resultant chest acceleration

Among the main factors, torso angle, right knee angle and left ankle angle have a significant effect on the response of peak resultant chest acceleration. Other factors, namely hip angle, left knee angle, right ankle angle and seatbelt pillar loop anchor height have negligible effects on peak resultant chest acceleration. While among the low order interactions, AC, AD, AF, AG are significant. Compared to the number of factors and interactions that have significant effects on HIC<sub>15</sub>, the total amount of significant factors and interactions for peak resultant chest acceleration is less. This could be partly explained by the fact that the response of HIC<sub>15</sub> is subjected to more body parts than peak chest resultant acceleration.

The formula of linear regression model for peak resultant acceleration is presented as following:

$$\begin{aligned}
 \text{Peak Resultant Chest Acceleration} = & 4.7547 + 0.2822 \text{ Torso Angle} - 0.0684 \text{ Hip Angle} \\
 & + 0.0059 \text{ Left Knee Angle} + 0.3628 \text{ Right Knee Angle} \\
 & - 0.2722 \text{ Left Ankle Angle} - 0.0141 \text{ Right Ankle Angle}
 \end{aligned}$$

$$\begin{aligned}
& - 0.1484 \text{ Seatbelt Anchor} - 0.0072 \text{ Torso Angle} * \text{Hip Angle} \\
& - 0.1903 \text{ Torso Angle} * \text{Left Knee Angle} \\
& + 0.2866 \text{ Torso Angle} * \text{Right Knee Angle} \\
& - 0.1222 \text{ Torso Angle} * \text{Left Ankle Angle} \\
& - 0.1678 \text{ Torso Angle} * \text{Right Ankle Angle} \\
& + 0.2866 \text{ Torso Angle} * \text{Seatbelt Anchor} \\
& + 0.1622 \text{ Hip Angle} * \text{Right Knee Angle} \\
& + 0.0347 \text{ Torso Angle} * \text{Hip Angle} * \text{Right Knee Angle}
\end{aligned}$$

Based on the linear regression model, estimation of effect of a specific factor could be computed through linear interpolation. One of the examples is the torso angle. Data shows that for one degree increase of torso angle, the relevant growth in peak chest resultant acceleration is 2.31%. And for right knee angle, the corresponding relation is 0.22% decrease of peak resultant chest acceleration to 1 degree increase of right knee angle. Similarly, effects of other factors and interactions could be determined though linear interpolation.

There is a disparity between the effect of left and right sides of body joint angles among the results. The right knee angle has a significant effect while the left knee angle does not, and the opposite is true for the right ankle and left ankle angle. The presence of the rigid gas paddle is a possible explanation. The right lower extremity is in contact with the rigid gas paddle at a desired knee and ankle angle at the very moment when the impact started. During the crash, the

right lower extremity acted as a support which resisted the motion of the upper body. The initial condition of such support could mostly likely change the mechanics of the upper body. However, it is not clear why the left ankle angle has a significant effect on peak resultant chest acceleration rather than the right ankle angle.

Compared to  $HIC_{15}$ , the peak resultant chest acceleration has fewer significant factors. Some of the variables that affect  $HIC_{15}$  do not have significant effect on the peak resultant chest acceleration. Such factors include hip angle and height of seatbelt pillar loop anchor. The analysis of variance of the data reveals that the height of seatbelt pillar loop anchor did affect the peak resultant chest acceleration. However, it is considered not significant when compared with other variables such as torso angle, right knee angle and left ankle angle. On the other hand, it is found that peak resultant chest acceleration is not sensitive to hip angle under such low impact speed (4.43 mph).

#### 4.3 Comparison of FE and Physical Test Results

An advantage of conducting FE along with physical experiments is the ability to compare results to further solidify the results. The difference between the results is the FE portion dealt with the main effects whereas the physical results dealt with a factorial design. Therefore, only the significance will be compared. For the  $HIC_{15}$ , it was found that the right knee and ankle are significant but the FE results include the left knee. Perhaps the impact speed for the physical experiment isn't high enough to cause an effect in the left knee.

As for the chest acceleration, the torso angle and left ankle angle agree with the FE results with the exception of the knee. For the physical results, the right knee is significant whereas the FE results for the left knee show a higher difference. There are major differences

between the FE and physical experiments, e.g. impact speed, actual vehicle vs. simplified sled, absence of arms, etc. The actual vehicle allows contact between dummy and vehicle interior. The addition of arms allows bracing not available to the simplified model. For the most part, the results are in agreement.

#### 4.4 THUMS Results

After running the baseline simulation, the results were compared with that of the FMVSS 208. The THUMS results match fairly well. The peak head acceleration of the THUMS is lower than that of the Hybrid III as shown in figure 4.17. The magnitude of incline slope of the two results are similar whereas the location of incline start differs. This could just be data collection discrepancy. The Hybrid III has a noticeable second peak right after the first peak. Their curve tails also differ noticeably.

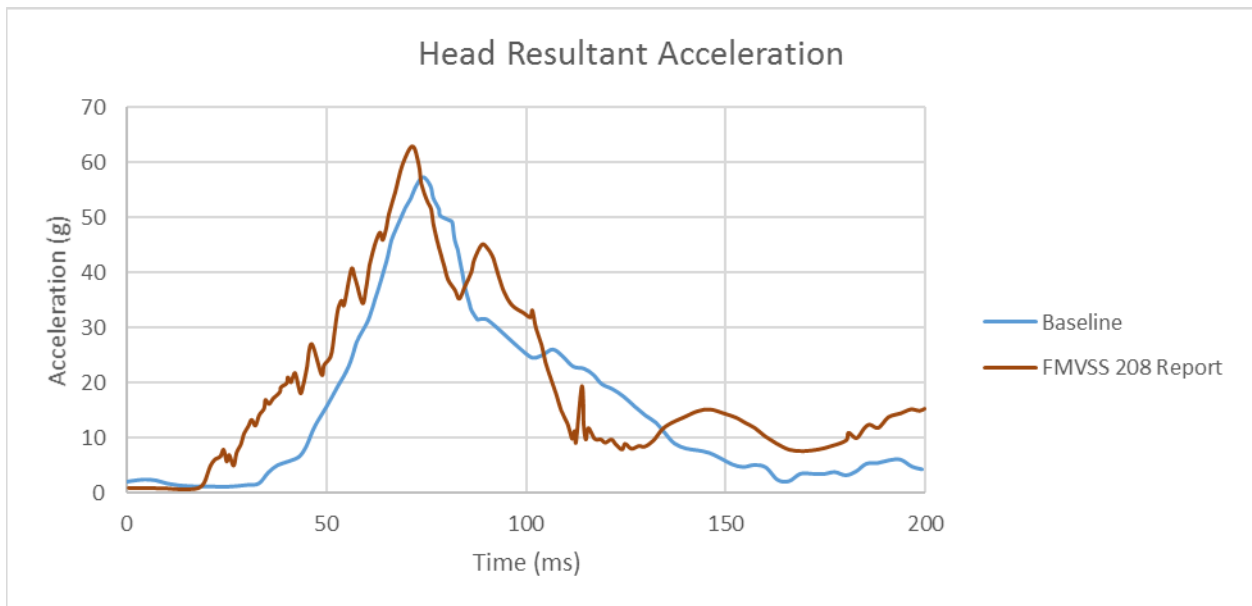


**Figure 4.17** Comparison of Head Acceleration between THUMS and FMVSS 208

As for the chest resultant acceleration, The THUMS result differs substantially from the FMVSS 208 report. The THUMS yielded lower accelerations all across the time duration of the crash.

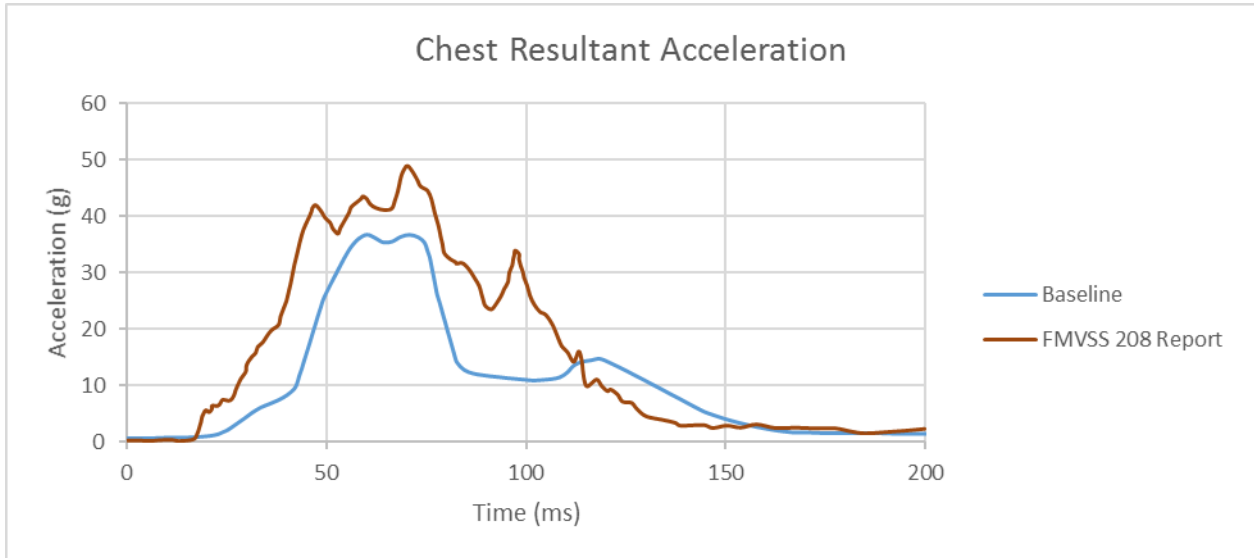


**Figure 4.18** Comparison of Chest Acceleration between THUMS and FMVSS 208

The injury criteria investigated with the THUMS were the head acceleration, chest acceleration, and chest deflection. The knees of the THUMS did not impact the knee bolster as shown in the crash before the head impacts the airbag, figure 4.19 therefore the femur forces were not investigated. Previously, the chest deflections were not investigated in the Hybrid III portion of the research. The pelvis acceleration was investigated previously but found to be insignificant compared to head and chest accelerations because of the frontal impact mode. Pelvis acceleration will not be investigated in the THUMS simulation.

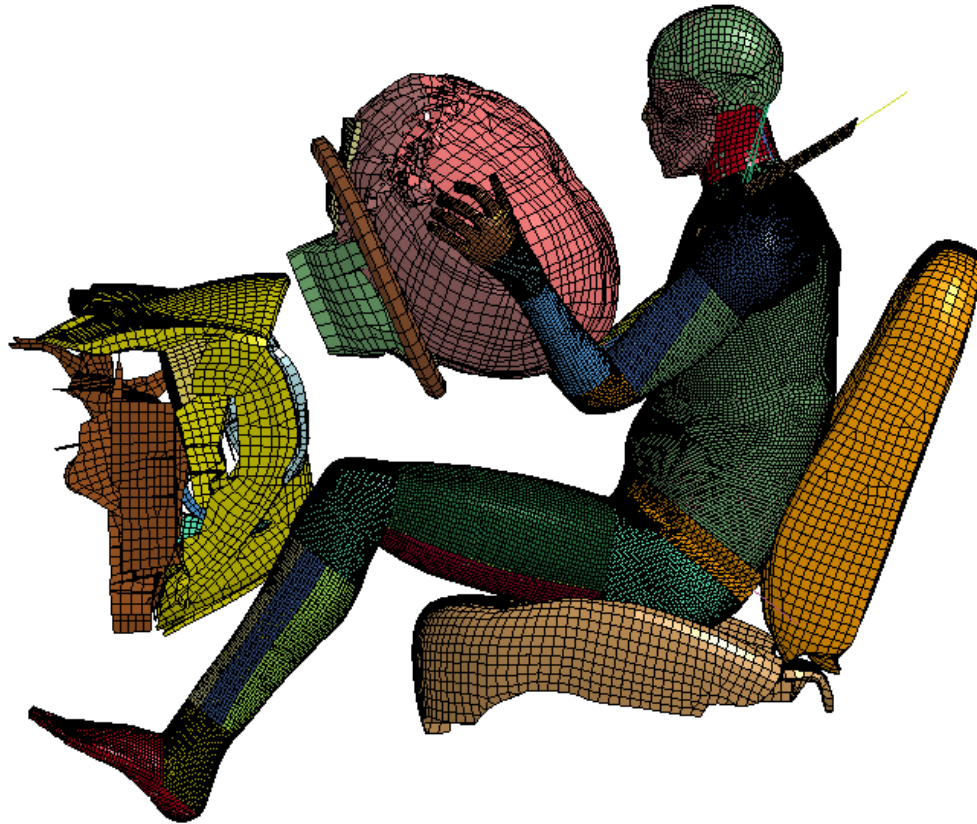


**Figure 4.19** THUMS Crash Simulation

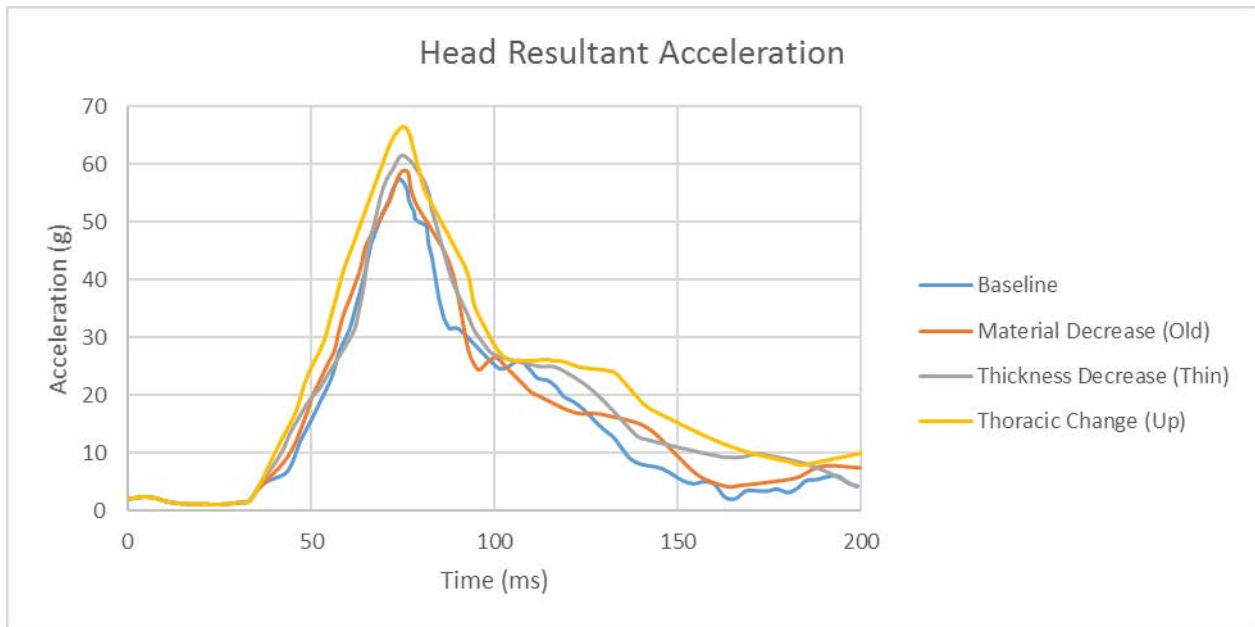


**Figure 4.20** THUMS Head Resultant Acceleration (Single)

The kyphosis effect thoracic change increased the head acceleration peak by as much as 8g. A substantial increase from the baseline is evident in figure 4.20. The decreased material property shows a slight increase from the baseline while the thinner bone thickness shows a larger increase than the decreased material property. Overall, the aging effects show increase head accelerations.

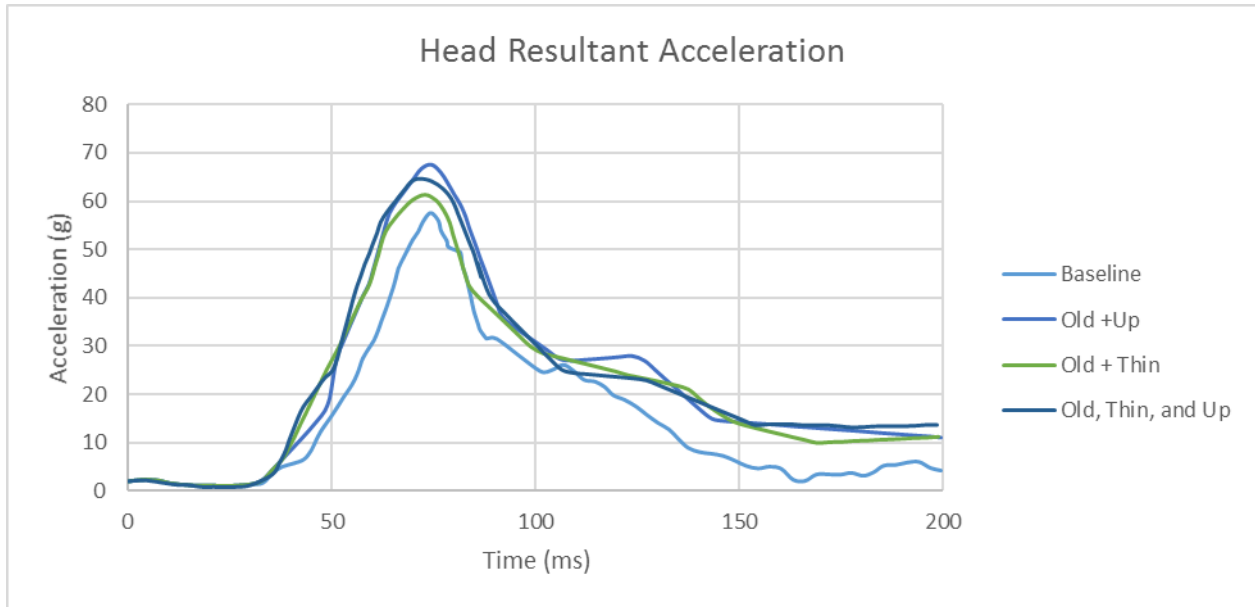


**Figure 4.21** THUMS Head Resultant Acceleration (Combinations)

The combinations of aging factors on the head acceleration also show increased values as shown in figure 4.21. The combination of old, thin, and up yield the highest peak value followed by the old and up combination. The old and thin combination shows the lowest increase in change.

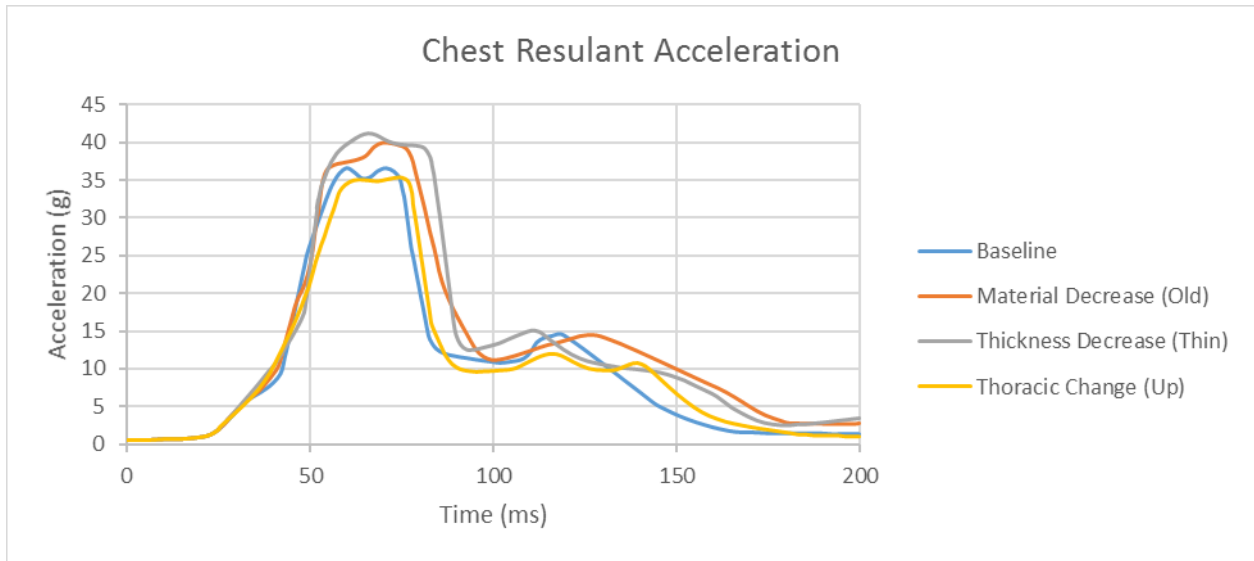


**Figure 4.22** THUMS Chest Resultant Acceleration (Single)

The kyphosis effect has an opposite effect on the chest acceleration. Instead of an increase in peak value, it remained the same as the baseline curve with a few variations. The first peak has a more constant (longer duration) acceleration and the second peak at 110 ms is than that of the baseline acceleration. Both the material property decrease and thickness decrease curves show noticeable increase in peak values. They also have similar acceleration at the second peak but at different times.

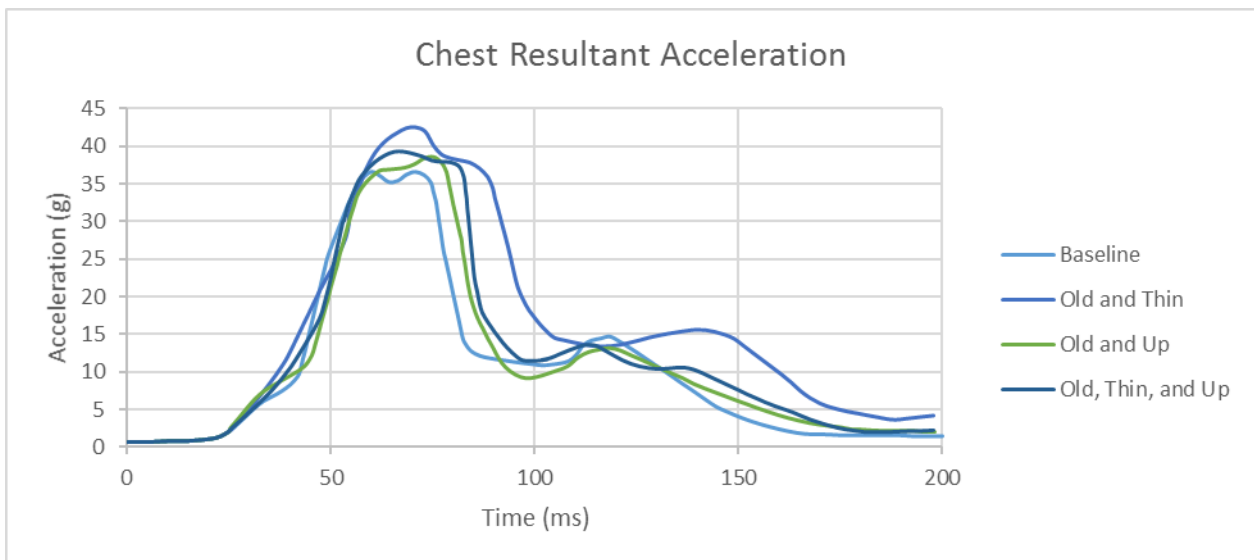


**Figure 4.23** THUMS Chest Resultant Acceleration (Combinations)

The aging factors affect the chest accelerations by allow the peak accelerations have a longer duration as evident in the figure 4.23. The combination of old, thin, and up yields the highest peak values and shows large changes. The first peak shows an increase of 5g than the baseline. The second peak is at a different time than the other combinations and it has a longer duration. The combination of old, thin, and up shows the second highest peak. The combination of old and up follows with a similar value but at a different location. Overall, all combinations show signs of increased acceleration from the baseline.



**Figure 4.24** THUMS Chest Deflection (Single)

The “kyphosis” aging effect shows a decrease of 3mm in chest deflection while the material propoerty decrease shows an increase by as much as 5mm. The thickness decrease shows an increase of 3mm. All the deflections follow similar a trend as shown in figure 4.24.

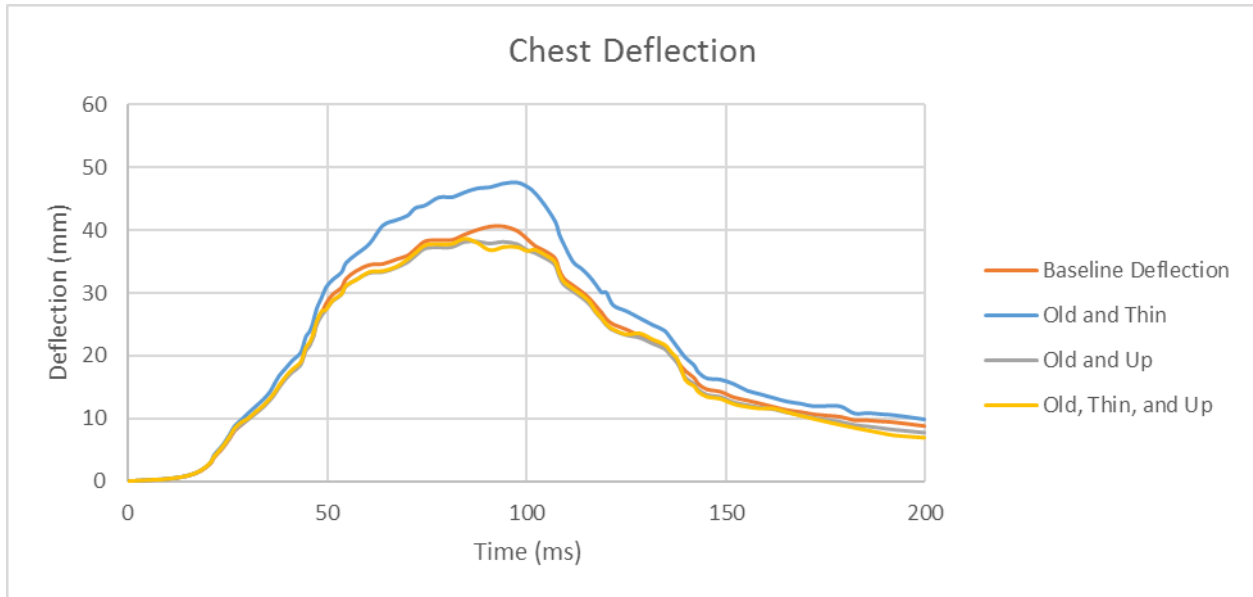


**Figure 4.25** THUMS Chest Deflection (Combinations)

As for the combinations show in figure 2.25, old and thin combination shows an increase in deflection as much as 8mm. The other two combinations are similar to that of the baseline deflection. It is evident that the “kyphosis” effect causes a decrease in deflection thus bringing the effect of the old and thin back down to the baseline. The “kyphosis” effect has a significant effect on the chest deflection rather the chest acceleration. Overall, the material property factor and compositional thickness factor have an increase effect on both the acceleration and deflection of the chest.

## Chapter 5 Conclusion/Future Work

### 5.1 Key Findings

Older drivers tend to sit closer to the steering wheel and exhibit contracted body joint angles compared to extended angles expressed by younger drivers who tend to be laid back in the driver’s seat. Using the finite element Hybrid III dummy model, we were able to come up with the main effects of posture changes affecting acceleration based injury criteria.

We conclude that sitting closer is actually beneficial for the Head Injury Criteria. When the driver's torso is contracted, hence closer to the wheel, the HIC will be 5% less than a younger driver who is more laid back into the seat. The young drivers with extended joints besides the torso joint yield HIC values as high as 19%. The extension of the arms and legs act as braces when they come into contact with the vehicle interior.

As for the chest acceleration, older drivers with contracted postures yield higher values. (Kent et al., 2005a) found that older drivers are more likely to die of a chest injury than a head injury. The chest acceleration is 3% higher for situations where the torso and left knee are contracted. Chest acceleration is dependent on seatbelt stiffness and slack. While the stiffness remains constant throughout all the simulations, there are differences in slack when the torso angle is changed. By contracting the torso, empty space can exist between the driver's back and seatback which can increase the baseline chest acceleration by 7%.

Comparing to the baseline values, changing posture does not affect the pelvis acceleration but comparing old postures with young postures, there are noticeable percent changes between them. The contracted postures with exception of left shoulder and right ankle are approximately 4-6% higher. In conclusion, old postures do not necessarily yield higher injury criteria values but in the case of contracted torso, all three injury criteria increase. Therefore, contracted torso commonly observed in older drivers is the most significant factor in increasing the injury possibility.

This investigation gave us an understanding of postures' effect on injury involving older occupants. With this knowledge, we can come up with engineering approaches to mitigate or

lessen injuries such as automatic contracting seatbacks that can sense incoming crash and conform to the older driver's back to brace for impact.

From the physical experiments, the torso angle, hip angle, right knee angle, right ankle angle and seatbelt pillar loop anchor location are found to be significant that affect the head injury criteria outcome. The extended torso angle (sitting further from steering wheel) yields a higher head injury criteria outcome. For the chest acceleration, the torso angle, right knee angle, and left ankle are significant.

From the THUMS simulations, it can be concluded that the "kyphosis" effect increases the head resultant acceleration. The thorax acts as the base of the neck that connects the head therefore it is reasonable that the changes in the thorax affects the head acceleration. The "kyphosis" effect decreases the deflection of the thorax because the ribs are more in line with the force imposed by the crash. It is able to withstand more force when the ribs are more parallel with the force. As for the chest acceleration, no significant change was present. The accelerometer is placed at the spine. The spine remains in the same position even with the kyphosis effect therefore the acceleration remains the same.

For the material property decrease, the chest deflection shows the highest increase. The head and chest accelerations show noticeable increases. For the bone compositional thickness decrease, the chest acceleration shows the highest increase. The head acceleration and chest deflection show noticeable increases. Overall with all three aging factors in place, the head and chest accelerations show high increases. Whereas for the deflection, it remains the same.

## 5.2 Recommendations and Future Work

The findings of the current work suggest that sitting closer to the steering wheel is actually beneficial for lessening head injury but more damaging for the thoracic. It is important to maintain a sensible driving posture that is neither too laid back nor too contracted to prevent severe injury. There is a possibility of sustaining lesser injury by exhibiting a particular posture therefore to mitigate injury of older drivers, there are some engineering approaches we can undertake such as better car seat design.

The development of an aged human model can provide us with the necessary tools for investigating detailed injuries. This information can help us improve occupant safety to prevent or lessen certain injuries. Future work may include looking into other modes of impact where certain relevant injury criteria will be looked at such as pelvis acceleration in side impact. Also, look into how we can use the aged human model to determine the lower injury tolerance older drivers have over younger drivers. Furthermore, with this new tool, we can focus on numerous occupant safety topics.

## References

- ANTONA, J., EJIMA, S. & ZAMA, Y. 2011. Influence of the Driver Conditions on the Injury Outcome in Front Impact Collisions. *International Journal of Automotive Engineering*, 2, 33-38.
- BALL, K., OWSLEY, C., SLOANE, M. & DANIEL, R., L. 1993. Visual Attention Problems as a Predictor of Vehicle Crashes in Older Drivers. *Invest Ophthalmol Vis. Sci.*, 34.
- BALL, K., OWSLEY, C., STALVEY, B., ROENKER, D. L., SLOANE, M. E. & GRAVES, M. 1998. Driving avoidance and functional impairment in older drivers. 30, 313–322.
- BOSE, D., CRANDALL, J. R., UNTAROIU, C. & MASLEN, E. 2010. Influence of pre-collision occupant parameters on injury outcome in a frontal collision. *Accident Analysis & Prevention*, 42, 1398-1407.
- BUREAU OF LABOR STATISTICS. 2013. *Labor Force Statistics from the Current Population Survey* Online. Washington, DC. Available: <http://www.bls.gov/cps/demographics.htm> Accessed.
- CENTER, T. C. S. R. 2011. *Developing new computer models to study the effects of automobile accidents on child and senior passengers* Online. Available: <http://www.toyota.com/csrf/finite-element-model-development-for-vulnerable-populations.html> Accessed 11/4/2014 2014.
- COURTNEY, A. C., HAYES, W. C. & GIBSON, L. J. 1996. Age-related differences in post-yield damage in human cortical bone. *Experiment and model*. 29, 1463–1471.
- EBY, D. W. & KANTOWITZ, B. H. 2006. *Human Factors and Ergonomics in Motor Vehicle Transportation*, Hoboken, NJ, John Willey & Sons.
- EL-JAWAHRI 2010. Development and Validation of Age-Dependent FE Human Models of a Mid-Sized Male Thorax. *Stapp Car Crash Journal*, 54, 25.
- EL-JAWAHRI, R. E., LAITURI, T. R., RUAN, J. S., ROUHANA, S. W. & BARBAT, S. D. 2010. Development and Validation of Age-Dependent FE Human Models of a Mid-Sized Male Thorax. *SAE Technical Paper*, 54, 25.
- EPPINGER, R., SUN, E., BANDAK, F., HAFFNER, M., KHAEWPOONG, N. & MALTESE, M. 1999. Development of Improved Injury Criteria for the Assessment of Advanced Automotive Restraint Systems - II. In: ADMINISTRATION, N. H. T. S. (ed.). *National Highway Traffic Safety Administration*.
- ERIKSSON, L. & KULLGREN, A. 2006. Influence of Seat Geometry and Seating Posture on NICmax Long-Term AIS 1 Neck Injury Predictability. *Traffic Injury Prevention*, 7, 61-69.

- FORMAN, J. L., KENT, R. W., MROZ, K., PIPKORN, B., BOSTROM, O. & SEGUI-GOMEZ, M. 2012. Predicting Rib Fracture Risk With Whole-Body Finite Element Models: Development and Preliminary Evaluation of a Probabilistic Analytical Framework. *Ann Adv Automot Med*.
- FRESSMANN, D. 2014. A parameterized geometry interpolation method for human body modeling. *LS-Dyna Conference*.
- FROST, H. M. 1997. On Our Age-Related Bone Loss: Insights from a New Paradigm. *Journal of Bone and Mineral Research*, 12.
- GAYZIK, F. S., LOFTIS, K. L., SLICE, D. E. & STITZEL, J. D. 2006. A Finite Element Study of Age-based Size and Shape Variation of the Human Rib Cage. *Biomedical Sciences Instrumentation*, 42, 10.
- GAYZIK, F. S., YU, M. M., DANIELSON, K. A., E., S. D. & D., S. J. 2008. Quantification of age-related shape change of the human rib cage through geometric morphometrics. 41, 1545–1554.
- GUHA, S. 2013. LSTC NCAC Hybrid III 50th Dummy. Michigan: Livermore Software Technology Corporation.
- HANSON, L., SPERLING, L. & AKSELSSON, R. 2006a. Preferred car driving posture using 3-D information. *International journal of vehicle design*, 42, 154-169.
- HANSON, L., SPERLING, L. & AKSELSSON, R. 2006b. Preferred car driving posture using 3-D information. *International Journal of Vehicle Design*, 42, 154-169.
- HERSHMAN & LAWRENCE, L. The U.S. New Car Assessment Program (NCAP): Past, Present, and Future. In: ADMINISTRATION, N. H. T. S. (ed.). National Highway Traffic Safety Administration.
- HERSHMAN, L. L. The US new car assessment program (NCAP): Past, present and future. International Technical Conference on the Enhanced Safety of Vehicles, 2001.
- HU, J., RUPP, J., D. & REED, M. P. 2012. Focusing on Vulnerable Populations in Crashes: Recent Advances in Finite Element Human Models for Injury Biomechanics Research. *Journal of Automotive Safety and Energy*, 3, 13.
- HUANG, M. 2002. *Vehicle Crash Mechanics*, Boca Raton, FL., CRC Press.
- HUMANETICS. 2014a. *Crash Test Dummies* Online. Plymouth, MI. Available: <http://www.humaneticsatd.com/crash-test-dummies> Accessed.
- HUMANETICS. 2014b. *Hybrid III 50th Male Dummy* Online. Humanetics Innovative Solutions. Available: <http://www.humaneticsatd.com/crash-test-dummies/frontal-impact/hybrid-iii-50th> Accessed 2014.

- ITO, D., EJIMA, S. & SUKEGAWA, Y. 2012. Assessment of Pre-crash Seatbelt Technology in Frontal Impacts Using a New Crash Test Sled System With Controllable Pre-impact Braking. *Japan Automobile Research Institute*, 13, 1-9.
- IVORY, M. & RICHARDSON, F. 2001. New Car Assessment Program Frontal Barrier Impact Test: 2002 Ford Explorer XLT 4WD SUV. *In: TRANSPORTATION*, U. S. D. O. (ed.). Washington, D.C.: U.S. Department of Transportation.
- IWAMOTO, M., NAKAHIRA, Y. & KIMPARA, H. 2010. Development of a Finite Element Model of 5th Percentile Female With Multiple Muscles and Its Application to Investigation on Impact Responses of Elderly Females. National Highway Traffic Safety Administration.
- KAHANE, C. J. 2013. Injury Vulnerability and Effectiveness of Occupant Protection Technologies for Older Occupants and Women. Washington, DC.
- KENT, R., HENARY, B. & MATSUOKA, F. 2005a. On the Fatal Crash Experience of Older Drivers. *Annu Proc Assoc Adv Automot Med*.
- KENT, R., LEE, S. H., DARVISH, K., WANG, S., POSTER, C. S., LANGE, A. W., BREDE, C., LANGE, D. & MATSUOKA, F. 2005b. Structural and material changes in the aging thorax and their role in crash protection for older occupants. *Stapp Car Crash J*, 49, 231-49.
- KIMPARA, H., LEE, J. B., YANG, K. H., KING, A. I., IWAMOTO, M., WATANABE, I. & MIKI, K. 2005. Development of a three-dimensional finite element chest model for the 5th percentile female. SAE Technical Paper.
- KYUNG, G. & NUSSBAUM, M. A. 2009. Specifying Comfortable Driving Posture for Ergonomics Design and Evaluation of the Driver Workspace Using Digital Human Models. *Ergonomics*, 52, 939-953.
- LEPORT, T., BAUDRIT, P., TROSSEILLE, X., PETIT, P., PALISSON, A. & VALLANCIEN, G. 2007. Assessment of the Pubic Force as a Pelvic Injury Criterion in Side Impact. *Stapp Car Crash J*, 51, 467-88.
- LSTC. 2014. *Hybrid III 50th Percentile Male* Online. Livermore, CA: Livermore Software Technology Corporation. Available: [http://www.lstc.com/products/models/dummies/H3\\_50th](http://www.lstc.com/products/models/dummies/H3_50th) Accessed.
- MARZOUGUI, D., BROWN, D., PARK, H. K., KAN, C. D. & OPIELA, K. S. 2013. Development & Validation of a Finite Element Model for a Mid-Sized Passenger Sedan. *13th International LS-DYNA Users Conference*.
- MARZOUGUI, D., SAMAHA, R., TAHAN, F., CUI, C. & KAN, C. 2012. Extended Validation of the Finite Element Model for the 2002 Ford Explorer Sport Utility Vehicle. *In: CENTER, T. N. C. A. (ed.)*. Ashburn, VA: The National Crash Analysis Center.

- MAURATH, C. & GUHA, S. 2010. Overview of LSTC's LS-DYNA Anthropomorphic Models. *11th International LS-DYNA Users Conference*. Dearborn, MI.
- MCCALDEN, R. W. 1993. Age-Related Changes in the Tensile Properties of Cortical Bone. The Relative Importance of Changes in Porosity, Mineralization, and Microstructure. *Journal of Bone & Joint Surgery*, 75.
- MCCOY, G., JOHNSTON, R. & DUTHIE, R. 1989. Injury to the elderly in road traffic accidents. *Journal of Trauma*, 494-497.
- MCPHERSON, G. 1980. The Elastic Modulus of Fetal Cranial Bone: A First Step Towards an Understanding of the biomechanics of Fetal Head Molding. *Journal of Biomechanics*, 13, 7.
- MELVIN, J. W., ROBBINS, D. H. & STALNAKER, R. L. Side Impact Response and Injury. 6th International Technical Conference on Experimental Safety Vehicles, 1976.
- MEYER, E. & HAUT, R. 2003. The Effect of Impact Angle on Knee Tolerance to Rigid Impacts. *Stapp Car Crash Journal*, 47, 1-19.
- MIZUNO, K., IWATA, K., DEGUCHI, T., IKAMI, T. & KUBOTA, M. 2005. Development of a three-year-old child FE model. *Traffic injury prevention*, 6, 361-371.
- MOHAN, P., PARK, C., MARZOUGUI, D., KAN, C., GUHA, S., MAURATH, C. & D., B. 2010. LSTC/NCAC Dummy Model Development. *11th International LS-DYNA Users Conference*. Dearborn, MI.
- MOORCROFT, D. M., STITZEL, J. D., DUMA, G. G. & DUMA, S. M. 2003. Computational model of the pregnant occupant: predicting the risk of injury in automobile crashes. *American journal of obstetrics and gynecology*, 189, 540-544.
- NALLA, R. K., KRUZIC, J. J., KINNEY, J. H. & RITCHIE, R. O. 2004. Effect of aging on the toughness of human cortical bone: evaluation by R-curves. *Bone*. United States.
- NCAC. 2014. *Finite Element Vehicle Model Archive* Online. Available: <http://www.ncac.gwu.edu/vml/models.html> Accessed.
- PARK, B. T., PARTYKA, S. C., MORGAN, R. M., HACKNEY, J. R., LEE, J., SUMMERS, L., LOWRIE, J. C. & BEUSE, N. M. 2000. Comparison of vehicle structural integrity and occupant injury potential in full-frontal and offset-frontal crash tests. SAE Technical Paper.
- PARK, J., EBERT, S. M., REED, M. P. & HALLMAN, J. J. 2015. Statistical models for predicting automobile driving postures for men and women including effects of age. *Human Factors: The Journal of the Human Factors and Ergonomics Society*, 0018720815610249.

- REED, M., EBERT, S. & HALLMAN, J. 2013. Effects of Driver Characteristics on Seat Belt Fit. *Stapp Car Crash Journal*, 57, 43-57.
- REED, M., EBERT, S. & RUPP, J. 2012. Effects of Obesity on Seat Belt Fit. *Traffic Inj Prev*, 13, 364-72.
- RUPP, J., REED, M., JEFFREYS, T. & SCHNEIDER, L. 2003. Effects of Hip Posture on the Frontal Impact Tolerance of the Human Hip Joint. *Stapp Car Crash J*, 47, 21-33.
- SAE, S. 2007. J211-1 Instrumentation for Impact Test—Part 1—Electronic Instrumentation. *SAE International*.
- SALZAR, R., BASS, C., KENT, R., MILLINGTON, DAVIS, M., LUCAS, S., RUDD, R., FOLK, B., DONNELLAN, L., MURAKAMI, D. & KOBAYASHI, S. 2006. Development of Injury Criteria for Pelvic Fracture in Frontal Crashes. *Traffic Injury Prevention*, 7, 299-305.
- SCHOELL, S. L. 2014. Development of age and sex-specific thorax finite element models. In: SYMPOSIUM, O. S. U. I. B. (ed.).
- STEIN, I. D. 1976. Rib structure and bending strength: an autopsy study. *Calcif Tissue Res*, 20, 61-73.
- TAMURA, A. 2015. Elderly Human Thoracic FE Model Development and Validation. *National Highway Traffic Safety Administration*.
- US CENSUS BUREAU. 2012. *Projections of the Population by Age and Sex for the United States: 2015 to 2060* Online. Washington, DC. Available: <http://www.census.gov/population/projections/data/national/2012/summarytables.html> Accessed.
- VICECONTI, M. 2004. Automatic generation of accurate subject-specific bone finite element models to be used in clinical studies. 37, 1597–1605.
- VICECONTI, M. & TADDEI, F. 2003. Automatic generation of finite element meshes from computed tomography data. *Crit Rev Biomed Eng*, 31, 27-72.
- YAMADA, H. 1970. *Strength of Biological Materials*, Baltimore, MD, Williams & Wilkins Company.
- YOGANANDAN, N., PINTAR, F. A., GENNARELLI, T. A., MALTESE, M. R. & EPPINGER, R. H. 2001. Mechanisms and factors involved in hip injuries during frontal crashes. *Stapp Car Crash J*, 45, 437-48.
- YUCESOY, C. 2002. Three-dimensional finite element modeling of skeletal muscle using a two-domain approach: linked fiber-matrix mesh model. 35, 1253–1262.

ZIOUPOS, P. & CURREY, J. D. 1998. Changes in the Stiffness, Strength, and Toughness of Human Cortical Bone With Age. *Bone*, 22, 57–66.